Title

CD24 signalling through macrophage Siglec-10 is a target for cancer immunotherapy

Permalink

https://escholarship.org/uc/item/2q04s1s6

Journal

Nature, 572(7769)

ISSN

0028-0836

Authors

Barkal, Amira A
Brewer, Rachel E
Markovic, Maxim
et al.

Publication Date

2019-08-01

DOI

10.1038/s41586-019-1456-0

Peer reviewed

CD24 signalling through macrophage Siglec-10 is a new target for cancer immunotherapy

Amira A Barkal[1,2,3,4], **Rachel E. Brewer**[1,2,3], **Maxim Markovic**[1,2,3,5], **Mark Kowarsky**[6], **Sammy A Barkal**[1], **Balyn W. Zaro**[1,2,3], **Venkatesh Krishnan**[8], **Jason Hatakeyama**[1,7], **Oliver Dorigo**[8], **Layla J Barkal**[9], **Irving L. Weissman**[1,2,3,10,*]

[1]Institute for Stem Cell Biology and Regenerative Medicine, Stanford University School of Medicine, Stanford, California 94305, USA

[2]Ludwig Center for Cancer Stem Cell Research and Medicine, Stanford University School of Medicine, Stanford, California 94305, USA

[3]Stanford Cancer Institute, Stanford University School of Medicine, Stanford, California 94305, USA

[4]Stanford Medical Scientist Training Program, Stanford University, Stanford, California 94305, USA

[5]Departments of Bioengineering and Applied Physics, Stanford University and Chan Zuckerberg Biohub, 318 Campus Drive, Stanford, CA 94305, USA

[6]Department of Physics, Stanford University, Stanford, CA, USA

[7]Department of Urology, Stanford University School of Medicine, Stanford CA 94305, USA

[8]Department of Obstetrics and Gynecology, Division of Gynecologic Oncology, Stanford University School of Medicine, Stanford, CA, USA

[9]Department of Medicine, Stanford University School of Medicine, Stanford, California 94305, USA

[10]Department of Pathology, Stanford University School of Medicine, Stanford CA 94305, USA

Summary:

Ovarian cancer and triple-negative breast cancer (TNBC) are among the most lethal diseases affecting women, with few targeted therapies and high rates of metastasis. Here we show that CD24 can be the dominant innate immune checkpoint in ovarian cancer and breast cancer, and is a new, promising target for cancer immunotherapy. Cancer cells are capable of evading clearance by macrophages through the overexpression of anti-phagocytic surface proteins, called "don't eat me" signals, including CD47[1], programmed cell death ligand 1 (PD-L1)[2], and the beta-2 microglobulin subunit of the major histocompatibility class I complex (B2M)[3]. Monoclonal antibodies which antagonize the interaction of "don't eat me" signals with their macrophage-expressed receptors have demonstrated therapeutic potential in several cancers[4–5]. However, variability in the magnitude and durability of the response to these agents has suggested the presence of additional, as yet unknown, "don't eat me" signals. Here we demonstrate a novel role for tumor-expressed CD24 in promoting immune evasion through its interaction with the inhibitory receptor, Sialic Acid Binding Ig Like Lectin 10 (Siglec-10), expressed by tumor-associated macrophages (TAMs). We observe that many tumors overexpress CD24 and that TAMs express high levels of Siglec-10. Both genetic ablation of CD24 or Siglec-10, and monoclonal antibody blockade of the CD24–Siglec-10 interaction, robustly augment the phagocytosis of all CD24-expressing human tumors tested. Genetic ablation as well as therapeutic blockade of CD24 resulted in a macrophage-dependent reduction of tumor growth and extension of survival, *in vivo*. These data highlight CD24 as a highly-expressed, anti-phagocytic signal in several cancers and demonstrate the therapeutic potential for CD24-blockade as cancer immunotherapy.

Main text:

CD24, also known as Heat Stable Antigen (HSA) or Small Cell Lung Carcinoma Cluster 4 Antigen, is a heavily glycosylated GPI-anchored surface protein [6–7] known to interact with Siglec-10 on innate immune cells in order to dampen damaging inflammatory responses to infection[8], sepsis[9], liver damage[10], and chronic graft versus host disease[11]. The binding of CD24 to Siglec-10 elicits an inhibitory signaling cascade mediated by SHP-1 and/or SHP-2 phosphatases associated with the two immunoreceptor tyrosine-based inhibition motifs (ITIMs) in the cytoplasmic tail of Siglec-10, thereby blocking TLR-mediated inflammation and the cytoskeletal rearrangement required for cellular engulfment by macrophages[12–14]. Studies have shown that CD24 is expressed by several solid tumors[15–16], however a role for CD24 in modulating tumor immune responses has not yet been shown. We thus sought to investigate whether CD24-mediated inhibition of the innate immune system could be harnessed by cancer cells as a mechanism to avoid clearance by macrophages expressing Siglec-10.

To assess the role of CD24–Siglec-10 signaling in regulating the macrophage-mediated immune response to cancer, we examined the expression of CD24 and Siglec-10 in various tumors and associated immune cells. RNA-sequencing data from TCGA and TARGET demonstrated high expression of CD24 in nearly all tumors analyzed (Extended Data Figure 1a, Tumor study abbreviations in Supplementary Table 1), as well as broad upregulation of CD24 expression in several tumors as compared to known innate immune checkpoints (Figure 1a). The greatest CD24 upregulation was observed in ovarian cancer (OV), over 9 log-fold; and, CD24 expression in TNBC was significantly higher than that in normal breast

or ER[+]PR[+] breast cancers (Extended Data Figure 1b,c). Stratification of patients by CD24 expression revealed increased relapse-free survival for ovarian cancer patients with lower CD24 expression, and an overall survival advantage for breast cancer patients with lower CD24 expression (Figure 1b,c). We investigated CD24 and Siglec-10 expression at a cellular level within the tumor by leveraging single-cell RNA-sequencing data from six primary samples of TNBC[17] (NCBI SRA: PRJNA485423, Figure 1d. Extended Data Figure 1d,e). TNBC cells exhibited robust expression of CD24, while all other cell clusters exhibited weak CD24 expression, thus illustrating the potential for CD24 as a tumor-specific marker (Figure 1d). A substantial fraction of TAMs were found to express Siglec-10, indicating the possibility for CD24–Siglec-10 interactions in TNBC (Figure 1d). CD24 expression was substantially higher than PD-L1 (CD274) in all patients analyzed (Extended Data Figure 1f), while CD47 was expressed highly by all cell types (Figure 1d). FACS analyses of primary human tumors revealed robust CD24 protein expression by breast cancer cells and ovarian cancer cells, and TAMs from both tumor types expressed Siglec-10 (Figure 1e,f, Extended Data Figure 2a). Human peritoneal macrophages obtained from patients without cancer expressed low levels of Siglec-10. (Extended Data Figure 2b). Analysis of PBMC subsets revealed low expression of Siglec-10 and CD24 by T cells, NK cells, and monocytes, whereas B cells were found to express modest levels of Siglec-10 and high levels of CD24 (Extended Data Figure 2c,d).

In order to investigate a role for CD24–Siglec-10 signaling in regulating the macrophage-mediated anti-tumor immune response (Figure 2a), we engineered a polyclonal subline of the normally CD24-positive MCF-7 human breast cancer cell line deficient in CD24 (ΔCD24). Although unstimulated (M0) human donor-derived macrophages expressed low levels of Siglec-10 by FACS, the addition of two inhibitory cytokines, TGFβ–1 and IL-10, induced robust expression of Siglec-10, indicating that Siglec-10 expression may be regulated by TAM-specific gene expression programs[18] (Extended Data Figure 2e). TGFβ–1,IL-10–stimulated (M2-like) macrophages were less phagocytic than unstimulated macrophages at baseline (Extended Data Figure 2f). We found that stimulation with the classic M2-polarizing cytokine, IL-4, was also sufficient to induce Siglec-10 expression. (Extended Data Figure 2g). Co-culture of either WT or ΔCD24 cells with M2-like macrophages expressing Siglec-10 revealed that CD24 deletion alone was sufficient to potentiate phagocytosis (Figure 2b). ΔCD24 cells were also significantly more sensitive to CD47 blockade (Clone 5F9-G4[19]), than WT cells, suggesting the cooperativity of combinatorial blockade of CD24 and CD47. To measure phagocytic clearance by automated live cell microscopy, GFP[+] WT and ΔCD24 cells were labeled with the pH-sensitive dye, pHrodo red[20], and co-cultured with macrophages. Over 36 hours, we found that ΔCD24 cells were more readily engulfed and degraded in the low-pH phagolysosome as compared to WT cells (Figure 2c).

Monoclonal antibody blockade of Siglec-10 augmented the phagocytic ability of macrophages, confirming a role for Siglec-10 in inhibiting phagocytosis (Figure 2d). In order to further investigate the impact of Siglec-10 expression on phagocytosis, we knocked out the *SIGLEC10* gene in donor-derived macrophages. We observed a dramatic reduction in Siglec-10 expression 72 h following electroporation with a single guide RNA (sgRNA) targeting the *SIGLEC10* locus, relative to cells electroporated with Cas9 alone (Cas9

control) (Figure 2e). Siglec-10 KO macrophages demonstrated significantly greater phagocytic ability than Cas9 control macrophages (Figure 2f).

Siglec-10 has been reported to interact with the highly sialylated form of CD24[13,14]. Accordingly, we observed that binding of Siglec-10-Fc to MCF-7 cells was significantly reduced upon surface desialylation (Figure 2g, Extended Data Figure 3b). This suggests that Siglec-10 has the capacity to recognize both protein and sialic acid ligands, and thus likely has varied ligands extending beyond CD24. Indeed, we observed that CD24 deletion alone is insufficient to completely abrogate Siglec-10-Fc binding in the presence of surface sialylation (Extended Data Figure 3a,b). However, in the absence of surface sialylation, Siglec-10-Fc binding was nearly abolished by CD24 deletion, suggesting that CD24 is the primary protein ligand for Siglec-10 (Figure 2h, Extended Data Figure 3b). We found that desialylation did not reduce the enhancement of phagocytosis observed with CD24 deletion, indicating that CD24 sialylation is not required to inhibit phagocytosis (Extended Data Figure 3c). Neither recombinant Siglec-5-Fc nor Siglec-9-Fc were found to bind CD24$^+$ MCF-7 cells, although both were expressed highly by donor-derived macrophages (Extended Data Figure 3d–g).

To investigate the possible human therapeutic potential of these findings, we examined whether direct monoclonal antibody (mAb) blockade of CD24 could enhance the phagocytosis of CD24$^+$ human cancers by disrupting CD24 –Siglec-10 signaling. (Extended Data Figure 4a). Automated live-cell microscopy revealed that MCF-7-pHRodo-Red$^+$ cells treated with a CD24 blocking mAb (clone SN3)[21] were more readily engulfed into the low pH phagolysosome, as demonstrated by enhanced red signal over time. (Figure 2i, Extended Data Figure 4b). Significant whole-cell phagocytosis was observed by confocal microscopy upon treatment with anti-CD24 mAb and dual blockade of both CD24 and CD47 further augmented cellular engulfment (Extended Data Figure 4c,d). Similarly, FACS-based measurements of phagocytosis revealed a robust increase in phagocytosis upon the addition of anti-CD24 mAb as compared to IgG control, greater than the effect observed with CD47 blockade (Figure 3a, Gating Scheme for *In Vitro* Phagocytosis in Extended Data Figure 5a). The response to anti-CD24 mAb was found to be dose-dependent and saturable (Extended Data 5b). CD24 blockade augmented the phagocytosis of all CD24-expressing cancers tested including breast cancer (MCF-7), pancreatic adenocarcinoma (Panc1), pancreatic neuroendocrine tumor (APL1), and small cell lung cancer (NCI-H82), and no effect was observed with CD24-cells (U-87 MG) (Figure 3b, Extended Data Figure 5c). Dual treatment with CD24 and CD47 blocking antibodies revealed an increased induction of phagocytosis to nearly 30-fold that of baseline in some cancers. Although CD47 genetic deletion did not alter the phagocytic susceptibility of MCF-7 cells on its own, upon treatment with anti-CD24 mAb,   CD47 cells were more readily engulfed than WT cells (Extended Data Figure 5d). Dual treatment of pancreatic adenocarcinoma cells with anti-CD24 mAb and Cetuximab, enhanced phagocytosis relative to either treatment alone, demonstrating potential synergy between anti-CD24 mAb and anti-solid tumor mAbs (Extended Data Figure 5e). An isotype-matched antibody against the surface marker EpCAM, expressed highly by MCF-7 cells, led to a modest increase in phagocytosis as compared to anti-CD24 mAb treatment, indicating the vast majority of the observed increase in phagocytosis upon the addition of anti-CD24 mAb is due to loss of CD24 signaling and not Fc-mediated

opsonization (Extended Data Figure 6a). Both M2-like and M0 macrophages were found to respond equally to opsonization by anti-EpCAM antibodies (Extended Data Figure 6b). Disruption of the interaction between the Fc portion of the anti-CD24 mAb and the Fc receptors, CD16 and CD32, led to a modest reduction in anti-CD24 mAb-induced phagocytosis, confirming that the Fc-mediated pro-phagocytic effect of the anti-CD24 mAb is minor (Extended Data Figure 6c).

All Siglec-10-expressing macrophages responded to CD24 blockade (Extended Data Figure 6d), and response magnitude trended towards a correlation with Siglec-10 expression (Extended Data Figure 6e). Genetic deletion of Siglec-10 led to dramatically reduced response to CD24 blockade, indicating that anti-CD24 mAb specifically disrupts CD24-Siglec-10 signaling (Figure 3c). Expression of CD24 correlated with response to CD24 blockade as well as with baseline phagoytosis levels, indicating tissue-specific expression of CD24 as a dominant "don't eat me" signal and highlighting the potential value for CD24 expression as a predictor of the innate anti-tumor immune response (Figure 3d, Extended Data Figure 6f).

Ovarian cancer cells were collected from patients with metastatic ovarian cancer and treated with anti-CD24 mAb in order to measure phagocytosis of *primary* human tumors. (Figure 3e). In these cases, CD24 blockade yielded a significantly greater effect than CD47 blockade, and dual treatment with both CD24 and CD47 blocking antibodies augmented phagocytosis at least additively (Figure 3f). Furthermore, anti-CD24 mAb treatment of primary human TNBC cells promoted phagocytic clearance by macrophages, while in these cases CD47 blockade had no effect on phagocytosis, indicating that anti-CD24 mAb may be efficacious in cancers demonstrating resistance to CD47 blockade (Extended Data Figure 6g).

To investigate whether the protection against phagocytosis conferred by CD24 could be recapitulated *in vivo*, GFP-luciferase[+] MCF-7 WT or MCF-7 CD24 cells were engrafted into NOD.Cg-Prkdc[SCID]Il2rg[tm1Wjl]/SzJ (NSG) mice[22]. Three weeks post-engraftment, we found that CD24-deficient tumors exhibited augmented levels of *in vivo* phagocytosis by infiltrating TAMs as compared to WT tumors, and TAMs infiltrating the CD24-deficient tumors also possessed a more inflammatory phenotype (Extended Data Figure 7, 8a–b). Over weeks, we observed a robust reduction of tumor growth of CD24 tumors as compared to WT tumors (Figure 4a,b). Importantly, the sub-lines assessed had no measurable cell-autonomous differences in proliferation *in vitro* (Extended Data Figure 8c). Notably, after 35 days of growth, the polyclonal CD24 tumors had become largely CD24^{+}, consistent with the selection against CD24^{−} cells by TAMs and the emergence of subclones of CD24^{+} cells that did not have biallelic CD24 deletion (Extended Data Figure 8d,e). TAM depletion did not significantly alter the burden of WT tumors, while loss of TAMs largely abrogated the reduction of tumor growth observed in CD24 tumors, indicating that increased TAM-mediated clearance of CD24 cells was responsible for the diminished tumor burden (Figure 4b, Extended Data Figure 8f). This growth difference due to enhanced phagocytic clearance resulted in a significant survival advantage for mice engrafted with CD24-deficient tumors (Figure 4c).

To determine whether the mouse homolog of human CD24, CD24a, could similarly confer protection against phagocytic clearance of cancer cells, we generated a subline of the mouse epithelial ovarian cancer line, ID8, lacking Cd24a (ID8 Cd24a). WT or Cd24a cells expressing GFP were injected intraperitoneally into NSG mice. After one week of growth, we observed that loss of CD24a was sufficient to significantly promote *in vivo* phagocytosis by NSG macrophages. (Extended Data Figure 9a). To assess the impact of CD24 in a syngeneic, fully immunocompetent setting, ID8 WT or ID8 Cd24a cells were engrafted intraperitoneally into C57Bl/6J mice. We observed that loss of CD24 was sufficient to dramatically reduce tumor growth over several weeks (Extended Data Figure 9b,c).

To demonstrate that enhancement of anti-tumor immunity could be modulated by therapeutic blockade of CD24, NSG mice with established MCF-7 WT tumors were treated with anti-CD24 monoclonal antibody for 2 weeks. Anti-CD24 monotherapy resulted in significant reduction of tumor growth compared to IgG control (Figure 4d,e, Extended Data Figure 9d).

Potential off-target effects of anti-CD24 mAb in humans include B cell depletion, due to high CD24 expression by B cells. Indeed, phagocytic clearance of healthy B cells was observed upon treatment with anti-CD24 mAb (Extended Data Figure 10a). However, we found that unlike anti-CD47 mAbs[4], the anti-CD24 mAb demonstrated no detectable binding to human red blood cells (RBCs), although mouse CD24a is expressed by mouse RBCs (Extended Data Figure 10b).

CD24 is a potent anti-phagocytic, "don't eat me," signal capable of directly protecting cancer cells from attack by Siglec-10-expressing macrophages. Monoclonal antibody blockade of CD24–Siglec-10 signaling robustly enhances clearance of CD24^{+} tumors, indicating promise for CD24 blockade as immunotherapy. Both ovarian cancer[23] and breast cancer have demonstrated weaker responses to anti-PDL-1/PD-1 immunotherapies than those observed in other cancers[24–26], suggesting that an alternate strategy may be required to achieve wide-ranging responses. It is notable that the "don't eat me" signals CD47, PD-L1, B2M, and now CD24, each involve ITIM-based macrophage signaling, which may indicate a conserved mechanism that leads to immunoselection of the subset of macrophage-resistant cancer cells, resulting in tumors that by nature avoid macrophage surveillance and clearance. CD24 expression may provide immediate predictive value on responsiveness to existing immunotherapies insofar as high CD24 expression may inhibit response to therapies reliant on macrophage function. Expression of CD24 and CD47 was found to be inversely related among Diffuse Large B cell Lymphoma (DLBCL) patients (Extended Data Figure 10c). The percentage of patients with CD24 over-expression compares well with the response rates observed with anti-CD47 + Rituximab combination therapy in DLBCL[4], opening the possibility that particular tumors might respond differentially to treatment with anti-CD24 and/or anti-CD47 mAbs. Determining the collective expression of pro- and anti-phagocytic signals expressed by cancers and associated macrophages could enable better prediction of responders and nonresponders. Collectively, this work defines CD24–Siglec-10 as a novel innate immune checkpoint critical for mediating anti-tumor immunity, and provides evidence for the therapeutic potential of CD24 blockade, with particular promise for the treatment of ovarian cancer and breast cancer.

Methods:

Statistics

Sample sizes were modeled after those from existing publications regarding *in vitro* immune killing assays and *in vivo* tumor growth assays, and an independent statistical method was not used to determine sample size. Statistical tests were performed in Graphpad Prism 8.

Human tumor bulk RNA-sequencing analysis

RNA-sequencing data regarding expression levels for CD24, CD274 (PD-L1), CD47, and B2M from human tumors and matched healthy tissues collected by The Cancer Genome Atlas (TCGA), the Therapeutically Applicable Research to Generate Effective Treatment Program (TARGET), and the Genotype-Tissue Expression Project (GTEX) were downloaded as log_2(Normalized counts +1) values from UCSC[27] (https://xenabrowser.net/) with the query "TCGA TARGET GTEX". Tumor types were filtered for those with 9 individual patients for either tumor or healthy tissues. In instances where there existed both TCGA matched normal tissues and GTEX normal tissues, all normal tissues were combined for analyses. Abbreviations for TCGA studies and number of samples analyzed are listed in Supplementary Table 1. Survival analysis was performed by stratifying patients into high or low CD24 expression using median expression values, and Kaplan-Meier plots were generated and analyzed using Prism 8. Two-dimensional contour plots were generated using Plotly (Plotly Technologies Inc.)

Single-cell RNA-sequencing analysis

Raw files from previously sequenced TNBC (accession PRJNA485423) were downloaded from the NCBI SRA (Karaayvaz et. al 2018[17]). The 1539 single-cell RNA-seq data was aligned to the human genome (GRCh38) using STAR (version 2.5.3a) and gene counts (gene models from ENSEMBL release 82) determined using htseq-count (intersection-nonempty mode, secondary and supplementary alignments ignored, no quality score requirement). The expression matrix was transformed to gene counts per million sequenced reads for each cell. High-quality cells were defined as those that had at least 200,000 cpm and at least 500 genes expressed. This resulted in 1001 cells.

Marker genes used in Karaayvaz et. al were used to determine cell types. This was done using UMAP (non-linear dimensionality reduction algorithm) on log-transformed cpm values for the marker genes and labeling each of the five clusters identified based on which cell markers were most expressed (see Extended Data Figure 1d). Scatter plots were made using this UMAP transformation with coloring as described in the figure legends.

Cell culture

All cell lines were purchased from ATCC with the exception of the APL1 cells, which were a gift from G. Krampitz (MD Anderson), and the ID8 cells, which were a gift from O. Dorigo. The human NCI-H82 and APL1 cells were cultured in RPMI+GlutaMax (Life Technologies) + 10% fetal bovine serum (FBS) + 100 U/mL penicillin/streptomycin (Life Technologies). Cell lines were not independently authenticated beyond the identity provided from ATCC. The human MCF-7, Panc1, and U87-GM cell lines were cultured in DMEM

+GlutaMax + 10% FBS + 100 U/mL penicillin/streptomycin. The murine ovarian carcinoma cell line, ID8, was cultured in DMEM + 4% FBS + 10% Insulin-Transferrin-Selenium (Corning) + 100 U/mL penicillin/streptomycin. All cells were cultured in a humidified, 5% CO_2 incubator at 37°C. All cell lines were tested for Mycoplasma.

Generation of MCF-7 and ID8 sub-lines

Parental MCF-7 and ID8 were infected with GFP-luciferase lentivirus in order to generate MCF-7-GFP-luc+ and ID8-GFP-luc+ cell lines, respectively. After 48 hours, cells were harvested and sorted by FACS in order to generate pure populations of GFP+ cells. The MCF-7/ CD24-GFP-luc+ and ID8/ Cd24a-GFP-luc+ sub-lines were generated by electroporating cells with recombinant CRISPR/Cas9 ribonucleoprotein (RNP), as described previously[5]. Briefly, CRISPR/Cas9 guide RNA molecules targeting human CD24 and mouse Cd24a, respectively, were purchased as modified, hybridized RNA molecules (Synthego) and assembled with Cas9-3NLS nuclease (IDT) via incubation at 37° for 45 minutes. Next, 2×10^6 MCF-7-GFP-luc+ or ID8-GFP-luc+ were harvested, combined with corresponding complexed Cas9/RNP and electroporated using the Lonza Nucleofector IIb using Kit V (VCA-1003). After 48 hours of culture, genetically-modified cells were harvested and purified through at least three successive rounds of FACS sorting in order to generate pure cell lines. Sequences for the guide RNA molecules used are, *hCD24* sgRNA: CGGUGCGCGGCGCGUCUAGC, hCD47 sgRNA: AAUAGUAGCUGAGCUGAUCC, and *mCd24a* sgRNA: AUAUUCUGGUUACCGGGAAA.

In vitro cell proliferation assay

Proliferation of the MCF-7 WT and MCF-7 CD24 cell lines was measured with live cell microscopy using an Incucyte (Sartorius). Cells were each plated at ~10% confluence. Percentage confluence following cell growth was measured as per manufacturers instructions every 8 h for 64 h.

Neuraminidase treatment and recombinant Siglec binding assay

MCF-7 cells were treated with either neuraminidase (from V*ibrio cholerae,* Roche) (1×10^6 cells/100U/mL) or neuraminidase that was heat inactivated for 15 min at 95 ° C prior to incubation for 1 h at 37° C in serum-free medium, after which reactions were quenched with serum prior to analysis. Recombinant Siglecs (10, 5, and 9) were purchased as human Fc-fusion proteins from R&D Systems. Binding of recombinant Siglecs versus human IgG1 control was assayed at a concentration of 1×10^5 cells/1 mg/mL at 37° C for 1 h, in the absence of EDTA. Cells were stained with a fluorescently-conjugated anti-human Fc antibody (Biolegend) to enable the measurement of recombinant Siglec binding by flow cytometry.

Macrophage generation and stimulation

Primary human donor-derived macrophages were generated as described previously[28]. Briefly, leukocyte reduction system (LRS) chambers from anonymous donors were obtained from the Stanford Blood Center. Peripheral monocytes were purified through successive density gradients using Ficoll (Sigma Aldrich) and Percoll (GE Healthcare). Monocytes

were then differentiated into macrophages by 7-9 days of culture in IMDM + 10% AB human serum (Life Technologies). Unless otherwise stated, macrophages used for all *in vitro* phagocytosis assays were stimulated with 50 ng/mL human TGFβ1 (Roche) and 50 ng/mL human IL-10 (Roche) on Days 3-4 of differentiation until use on Days 7-9. IL-4 stimulation was added at a concentration of 20 ng/mL on Days 3-4 of differentiation until use on Days 7-9.

Human macrophage knockouts

Genetic knockouts in primary human donor-derived macrophages were performed as described previously[5]. Briefly, sgRNA molecules targeting the first exon of *SIGLEC10* were purchased from Synthego as modified, hybridized RNA molecules. The *SIGLEC10* sgRNA sequence used is: AGAAUCUCCCAUCCAUAGCC. Mature (day 7) donor-derived macrophages were electroporated with Cas9 ribonuclear proteins using the P3 Primary Cell Nucleofection Kit (Lonza V4XP-3024). Macrophages were harvested for analysis and functional studies 72 hours after electroporation. Indel frequencies were quantified using TIDE software as described previously[29].

Human samples

The Human Immune Monitoring Center Biobank, the Stanford Tissue Bank, Dr. Oliver Dorigo, and Dr. Gerlinde Wernig all received IRB approval from the Stanford University Administrative Panels on Human Subjects Research and complied with all ethical guidelines for human subjects research to obtain patient samples of ovarian cancer and breast cancer, and received informed consent from all patients. Single cell suspensions of solid tumor specimens were achieved by mechanical dissociation using a straight razor, followed by an enzymatic dissociation in 10 mL of RPMI + 10 μg/mL DNaseI (Sigma Aldrich) + 25 μg/mL Liberase (Roche) for 30-60 min at 37°C with vigorous pipetting every 10 minutes to promote dissociation. After a maximum of 60 min, dissociation reactions were quenched with 4°C RPMI + 10% FBS and filtered through a 100 micron filter and centrifuged at 400 g for 10 min at 4°C. Red blood cells in samples were then lysed by resuspending tumor pellet in 5 mL ACK Lysing Buffer (Thermo Fisher Scientific) for 5 min at RT. Lysis reactions were quenched by the addition of 20 mL RPMI + 10% FBS, and samples were centrifuged at 400 g for 10 min at 4°C. Samples were either directly analyzed, or resuspended in Bambanker (Wako Chemicals USA), aliquoted into cryovials and frozen prior to analysis.

FACS of primary human tumor samples

Single cell suspensions of primary human samples were obtained (described above), and frozen samples were thawed for 3-5 min at 37°C, washed with DMEM + 10% FBS, and centrifuged at 400 g for 5 min at 4°C. Samples were then resuspended in FACS buffer at a concentration of 1 million cells per mL and blocked with monoclonal antibody to CD16/32 (Trustain fcX, Biolegend) for 10-15 minutes on ice prior to staining with antibody panels. Antibody panels are listed below, with clones, fluorophores, usage purpose, and concentrations used listed in Supplementary Table 2. Samples were stained for 30 min on ice, and subsequently washed twice with FACS buffer, and resuspended in buffer containing 1 μg/mL DAPI prior to analysis. Fluorescence compensations were performed using single-stained UltraComp eBeads (Affymetrix). Gating for immune markers and DAPI was

performed using fluorescence minus one controls, while CD24^{+} and Siglec-10^{+} gates were drawn based off of appropriate isotype controls (See Extended Data Figure 2a for gating strategy). Flow cytometry was performed either on a FACSAria II cell sorter (BD Biosciences) or on an LRSFortessa Analyzer (BD Biosciences) and all flow cytometry data reported in this work was analyzed using FlowJo. Human tumor gating schemes were as follows:

Human TAMs: DAPI^{−}, EpCAM^{−}, CD14^{+}, CD11b^{+}

Human Tumor cells: DAPI^{−}, CD14^{−}, EpCAM^{+}

Flow cytometry-based phagocytosis assay

All *in vitro* phagocytosis assays reported here were performed by co-culture target cells and donor-derived macrophages at a ratio of 100,000 target cells to 50:000 macrophages for 1-2 h in a humidified, 5% CO_2 incubator at 37°C in ultra-low-attachment 96-well U-bottom plates (Corning) in serum-free IMDM (Life Technologies). Cells with endogenous fluorescence were harvested from plates using TrypLE Express (Life Technologies) prior to co-culture. Cell lines lacking endogenous fluorescence, NCI-H82 and Panc1, were harvested using TrypLE Express and fluorescently labeled with Calcein AM (Invitrogen) by suspending cells in PBS + 1:30,000 Calcein AM as per manufacturer instructions for 15 min at 37°C and washed twice with 40 mL PBS before co-culture. For TNBC primary sample phagocytosis assays, tumors were acquired fresh on the day of resection and dissociated as described above. EpCAM+ tumor cells were purified on an autoMACS pro separator (Miltenyi) by first depleting samples of myeloid cells using anti-CD14 microbeads (Miltenyi, 1:50) followed by an enrichment with anti-EpCAM microbeads (Miltenyi, 1:50). For primary ovarian cancer ascites assays, ovarian ascites samples were frozen as described above, thawed, and directly labeled with Calcein-AM (Invitrogen) at a concentration of 1:30,000. For primary B cell phagocytosis assays, B cells were enriched from pooled donor PBMC fractions using an autoMACS pro separator (Miltenyi) using anti-CD19 microbeads (Miltenyi, 1:50). For Fc-receptor blockade phagocytosis assays, macrophages were pre-treated with 10 μg/mL human Fc receptor blocking solution (BioLegend) for 45 minutes at 4°C , and subsequent co-culture with mAb-treated target cells was conducted in the presence of 10 μg/mL human Fc receptor blocking solution. For all assays, macrophages were harvested from plates using TrypLE Express. For phagocytosis assays involving treatment with monoclonal antibodies including anti-CD24 (Clone SN3, Novus Biologics) and anti-CD47 (Clone 5F9-G4, acquired from Forty Seven Inc.), all antibodies or appropriate isotype controls were added at a concentration of 10 μg/mL. After co-culture, phagocytosis assays were stopped by placing plates on ice, centrifuged at 400 g for 5 min at 4°C and stained with A647-labeled anti-CD11b (Clone M1/70, Biolegend) to identify human macrophages. Assays were analyzed by flow cytometry on an LRSFortessa Analyzer (BD Biosciences) or a CytoFLEX (Beckman) both using a high-throughput auto-sampler. Phagocytosis was measured as the number of CD11b+, GFP+ macrophages, quantified as a percentage of the total CD11b+ macrophages. Each phagocytosis reaction (independent donor and experimental group) was performed in a minimum of technical triplicate, and outliers were removed using GraphPad Outlier Calculator (http://graphpad.com/quickcalcs/Grubbs1.cfm).

In order to account for innate variability in raw phagocytosis levels among donor-derived macrophages, phagocytosis was normalized to the highest technical replicate per donor. All biological replicates indicate independent human macrophage donors. See Supplementary Table 2 for antibodies and isotype controls used in this study, and Extended Data Figure 5a for example gating. Response to anti-CD24 mAb was computed by the phagocytosis fold change between anti-CD24 mAb treatment and IgG control.

Time-lapse live-cell microscopy-based phagocytosis assay

Non-fluorescently labeled MCF-7 cells were harvested using TrypLE express and labeled with pHrodo Red, SE (Thermo Fisher Scientific) as per manufacturer instructions at a concentration of 1:30,000 in PBS for 1 h at 37°C, followed by two washes with DMEM + 10% FBS + 100 U/mL penicillin/streptomycin. Donor-derived macrophages were harvested using TrypLE express and 50,000 macrophages were added to clear, 96-well flat-bottom plates and allowed to adhere for 1 h at 37°C. After macrophage adherence, 100,000 pHrodo-Red-labeled MCF-7 cells + 10 μg/mL anti-CD24 antibody (SN3) were added in serum-free IMDM. The plate was centrifuged gently at 50 g for 2 min in order to promote the timely settlement of MCF-7 cells into the same plane as adherent macrophages. Phagocytosis assay plates were then placed in a 37°C incubator and imaged at 10-20 minute intervals using an Incucyte (Essen). The first image time point (reported as t = 0) was generally acquired within 30 minutes after co-culture. Images were acquired using a 20× objective at 800 ms exposures per field. Phagocytosis events were calculated as the number of pHrodo-red+ events per well and values were normalized the maximum number of events measured across technical replicates per donor. Thresholds for calling pHrodo-red+ events were made based off intensity measurements of pHrodo-red-labeled cells lacking any macrophages.

High-resolution phagocytosis microscopy

Fluorescently labeled MCF-7 cells (mCherry[+]) and donor-derived macrophages were harvested as described above. Suspensions consisting 50,000 macrophages and 100,000 MCF-7 cells + 10 μg/mL antibody or isotype control in serum-free IMDM were placed into an untreated 24-well plate, in order to allow for adherence of donor-derived macrophages, while preventing MCF-7 adherence. Reactions were incubated for 6 hours in a 37°C incubator. Following the incubation, wells were washed vigorously five times with serum-free IMDM in order to wash away non-phagocytosed MCF-7 cells. Whole-cell phagocytosis was evaluated using the Leica DMI 6000B fluorescent microscope and the Olympus IX83. High-resolution *z*-stack images were taken on the Zeiss LSM800 confocal microscope. All images were processed in ImageJ and Adobe Illustrator.

Mice

NOD.Cg-*Prkdc^scid^Il2rg^tm1Wjl^*/SzJ (NSG) mice were obtained from in-house breeding stocks. C57Bl/6J mice were obtained from Jackson Laboratory. All experiments were carried out in accordance with ethical care guidelines set by the Stanford University Administrative Panel on Laboratory Animal Care (APLAC). In compliance with Stanford APLAC protocol (26270), mice in long-term tumor studies were continually monitored to ensure adequate body condition scores and that tumors were less than 2.5cm in diameter and

50% ulceration. Female mice were used for all studies. Investigators were not blinded for animal studies.

In vivo phagocytosis analysis

For ID8 peritoneal phagocytosis analysis, 4×10^6, ID8-WT-GFP-luc+ cells or ID8- Cd24a-GFP-luc+ cells were engrafted into 6-8 week old female NSG mice via intraperitoneal injection of single cell suspensions in PBS. After 7 days, cells were harvested by peritoneal lavage. For MCF-7 xenograft phagocytosis analysis, female NSG mice, 6-10 weeks of age, were engrafted with 4×10^6 MCF-7-WT-GFP-luc+ cells or MCF-7-MCF-7- CD24-GFP-luc + cells by injection of single cell suspension in 25% Matrigel Basement Membrane Matrix (Corning) + 75% RPMI orthotopically into the mammary fat pad. Tumors were allowed to grow for 28 days after which tumors were resected and dissociated mechanically and enzymatically as described above. Single-cell suspensions of tumors were blocked using anti-CD16/32 (mouse TruStain FcX, BioLegend) for 15 min on ice as described above, prior to staining. Phagocytosis was measured as the percentage of CD11b$^+$, F4/80$^+$ TAMs that were also GFP+ (See Extended Data Figure 7 for example gating). Mouse TAM gating schemes were as follows:

Mouse TAMs: DAPI$^-$, CD45$^+$, CD11b$^+$, F480$^+$

M1-like Mouse TAMs: DAPI$^-$, CD45$^+$, CD11b$^+$, F480$^+$, CD80$^+$

In vivo xenograft tumor growth experiments

Female NSG mice, 6-10 weeks of age, were engrafted with 4×10^6 MCF-7-WT-GFP-luc+ cells or MCF-7- CD24-GFP-luc+ cells as described above. Tumors were measured using bioluminescence imaging (BLI) beginning 7 days post-engraftment and continuing every 7 days until Day 28. Animals were injected intraperitoneally with D-firefly Luciferin at 140mg/kg in PBS and images were acquired 10 minutes after luciferin injection using an IVIS Spectrum (Perkin Elmer). Total flux was quantified using Living Image 4.0 software. For survival analyses, animal deaths were reported as the days when primary tumor burden reached 2.5 cm and/or body condition scoring (BCS) values fell below that allowed by our animal protocols.

### *In vivo* macrophage depletion treatment study

Female NSG mice, 6-10 weeks of age were depleted of macrophages as described previously[4] by treatment with 400 μg CSF1R antibody per mouse or PBS (vehicle) (BioXCell, Clone AFS98) three times per week for 18 days prior to engraftment, and throughout the duration of the experiment. Successful tissue resident macrophage depletion was confirmed by flow cytometry prior to tumor engraftment by peritoneal lavage and flow cytometry analysis (Extended Data Figure 8f). Macrophage-depleted animals or vehicle treated animals were randomized prior to being engrafted with either MCF-7-WT-GFP-luc+ or MCF-7- CD24-GFP-luc+ cells as described above.

Immunocompromised tumor treatment studies

6-8 week old female NSG mice were engrafted with 4×10^6 MCF-7-WT-GFP-luc+ cells. Day 5 post-engraftment, total flux of all tumors was measured using bioluminescence imaging and engraftment outliers were removed using GraphPad Outlier Calculator. Mice were randomized into treatment groups, receiving either anti-CD24 monoclonal antibody (clone SN3, Creative Diagnostics) or mouse IgG1 isotype control (clone MOPC-21, BioXcell). On day 5 post-engraftment, mice received an initial dose of 200 μg and were subsequently treated every other day at a dose of 400 μg for 2 weeks. Bioluminescence imaging was performed throughout the study and after treatment withdrawl in order to assess tumor growth.

***In vivo* immunocompetent growth experiments**—Female C57Bl/6 mice, 6-8 weeks of age were injected intraperitoneally with 1×10^6 ID8-WT-tomato-luc+ or ID8- Cd24a-tomato-luc+ cells in PBS. Tumor growth was measured by weekly bioluminescence imaging beginning two weeks post-engraftment.

Extended Data
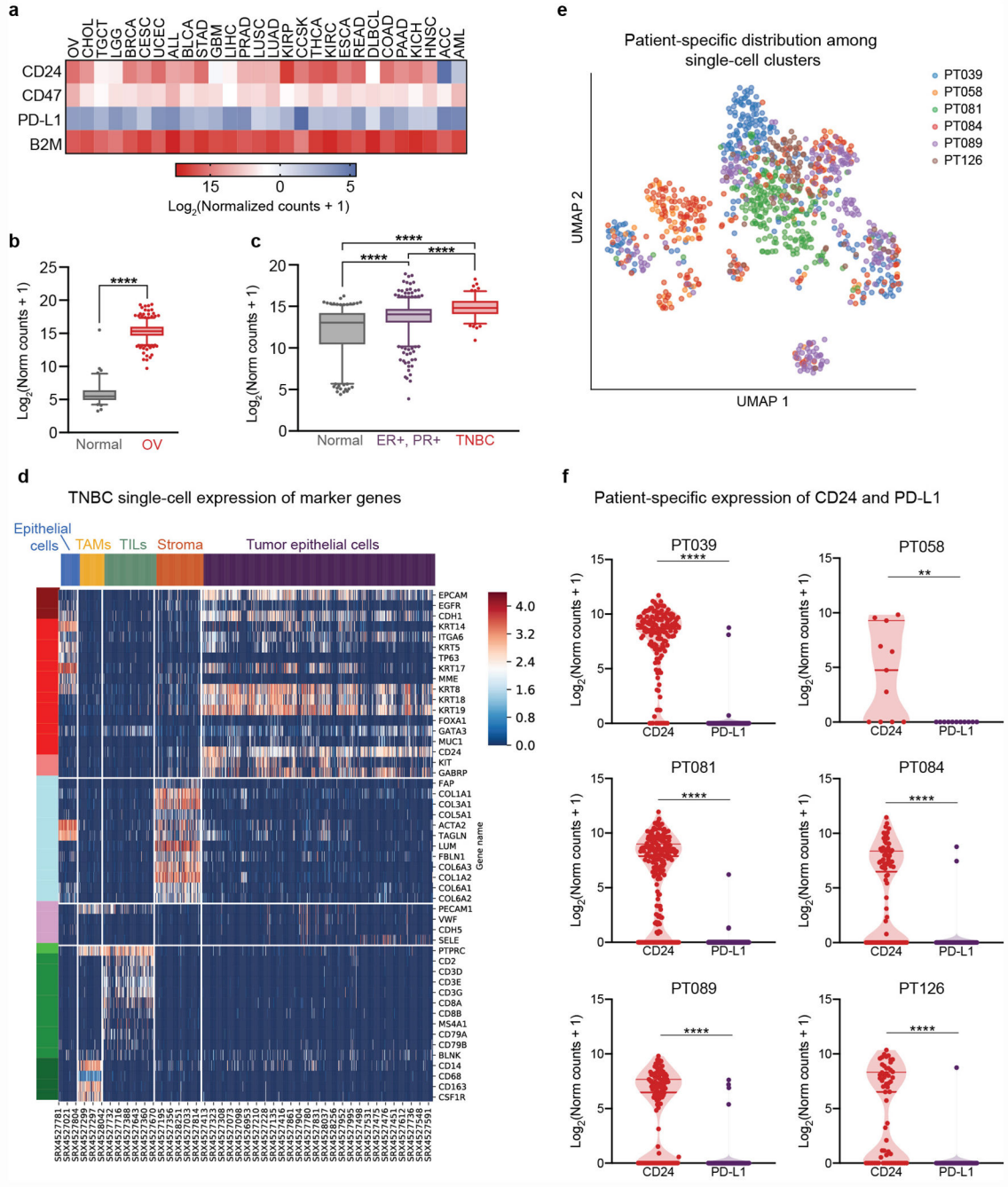
Extended Data Figure 1.

Expression of innate immune checkpoints in human cancer

a, Heatmap of expression (log$_2$(Normalized counts + 1)) of CD24 from bulk TCGA/TARGET studies, as compared to known innate immune checkpoint molecules, CD47, PD-L1, and B2M (tumor study abbreviations and n defined in Supplementary Table 1). **b,** Expression levels of CD24 in ovarian cancer (OV, red boxplot, $n = 419$) in comparison with ovarian tissue from healthy individuals (gray boxplot, $n = 89$), boxes show the median and whiskers indicate the 95th and 5th percentiles, ****P<0.0001, unpaired, two-tailed Student's

t-test. **c,** Expression levels of CD24 in TNBC (red boxplot, n = 124) in comparison with ER$^+$PR$^+$ breast cancer (ER$^+$PR$^+$, purple boxplot, $n = 508$) and normal breast (gray boxplot, $n = 293$). Each symbol represents an individual patient sample, boxes show the median and whiskers indicate the 95th and 5th percentiles, ****P<0.0001, one-way ANOVA with multiple comparisons correction, $F_{(2,922)} = 95.80$. **d,** Heatmap of marker gene expression (y-axis) across TNBC single cells (x-axis) and cell clusters identified (top). **e,** UMAP dimension 1 and 2 plots displaying all TNBC cells analyzed from six patients ($n = 1001$ single cells); cell clusters are colored by cell patient (key, left). **f,** CD24 vs. PD-L1 expression in the "Tumor epithelial cell" cluster for individual TNBC patients; number of single cells analyzed, PT039 $n = 151$ cells, PT058 $n = 11$ cells, PT081 $n = 196$ cells, PT084 $n = 84$ cells, PT089 $n = 117$, PT126 $n = 60$ cells. **P<0.01, ****P<0.0001. Data are violin plots showing median expression (log$_2$(Norm counts +1) and quartiles (paired, two-tailed *t*-test).
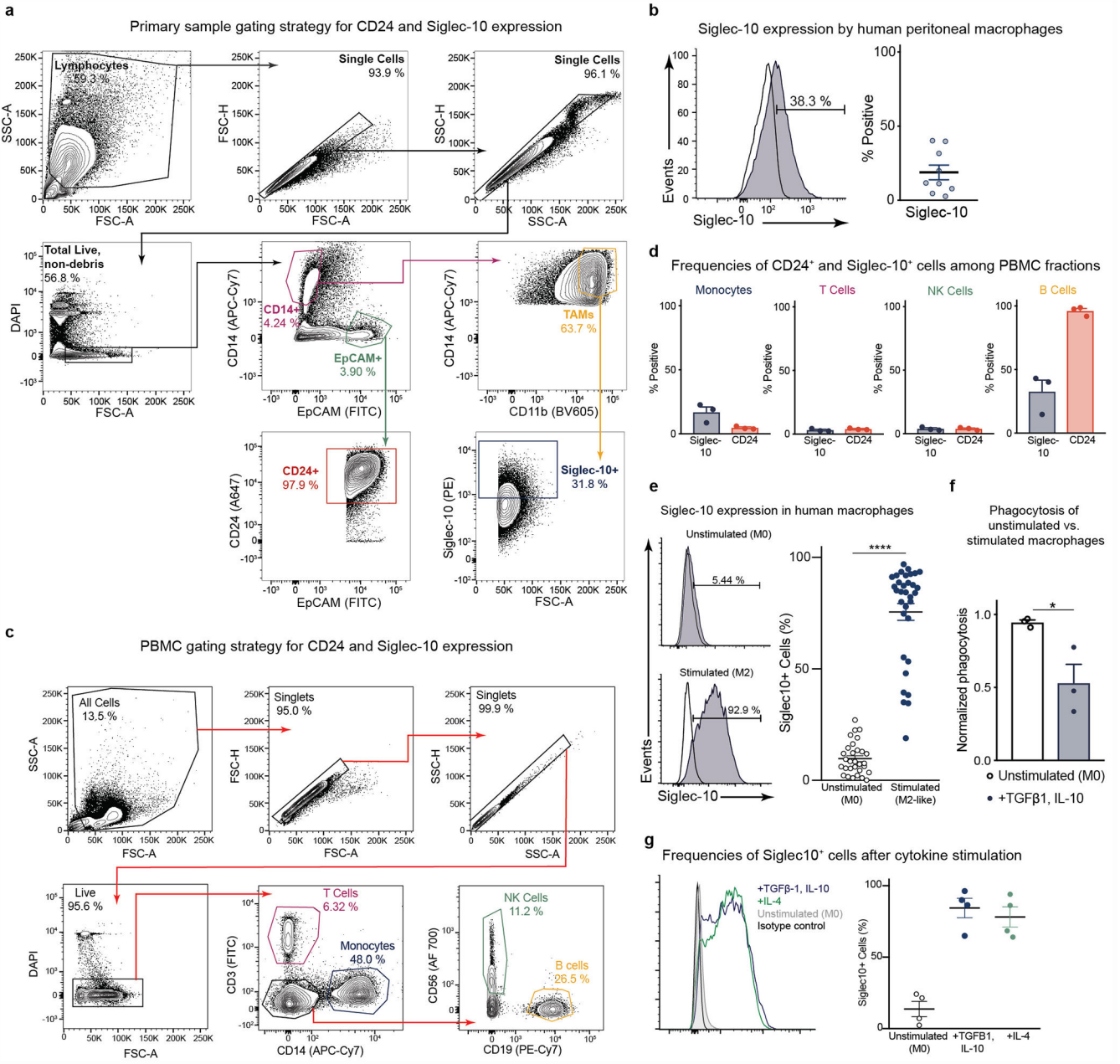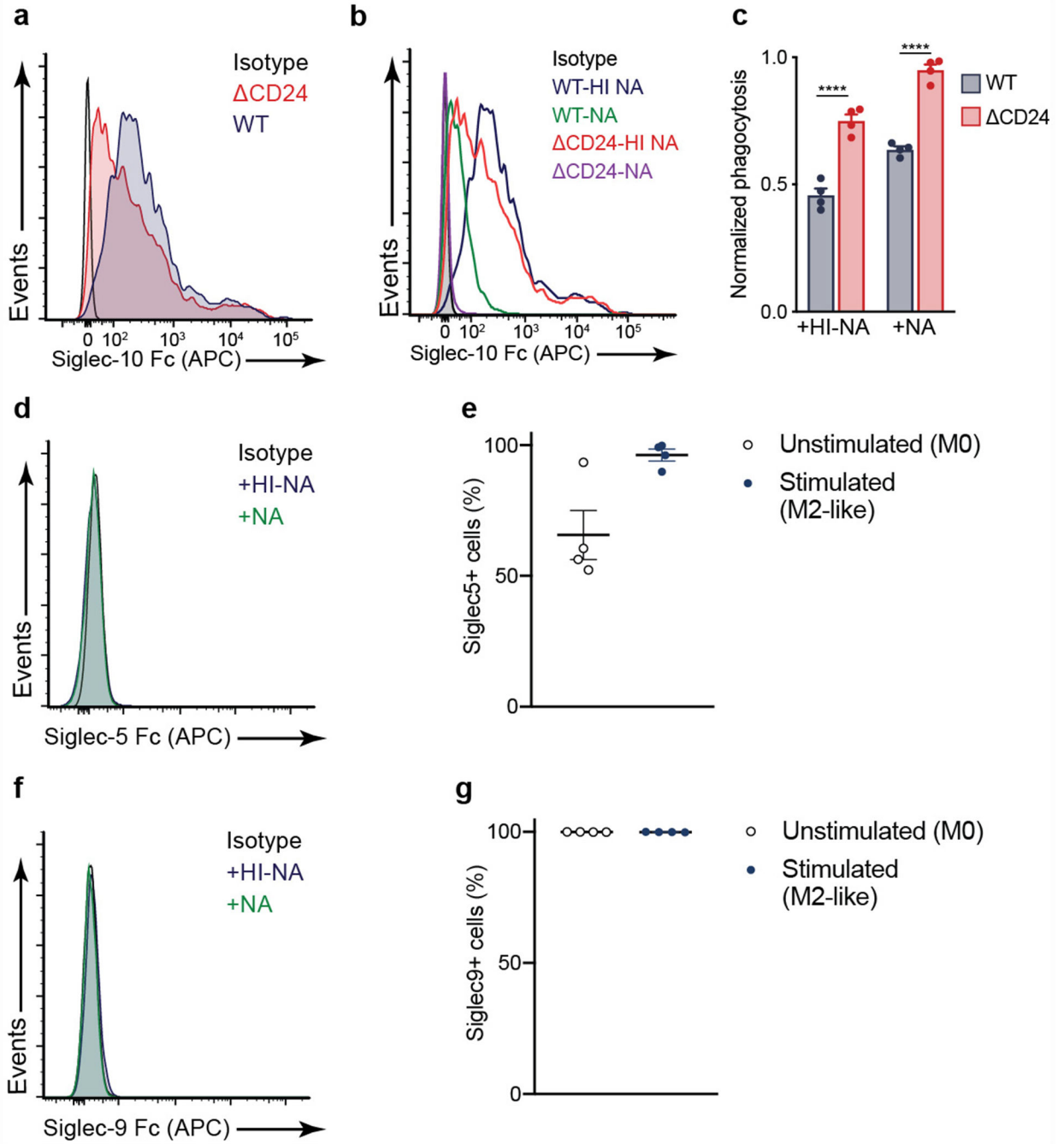
Extended Data Figure 2.

Flow-cytometry analysis of CD24 and Siglec-10 expression in human tumors and primary immune cells

a, Gating strategy for CD24+ cancer cells and Siglec-10+ TAMs in primary human tumors; after debris and doublet removal, cancer cells were assessed as DAPI−CD14− EpCAM+ and TAMs were assessed as DAPI−EpCAM−CD14+CD11b+. Plots are representative of 6 experimental replicates. **b,** (top) Representative flow cytometry histogram measuring the expression of Siglec-10 (blue shaded curves) versus isotype control (black lines) by non-cancerous peritoneal macrophages, numbers above bracketed line indicate percent macrophages positive for expression of Siglec-10; (bottom) frequency of peritoneal

macrophages positive for Siglec-10 among all peritoneal macrophages as defined by isotype controls ($n = 9$ donors). **c,** Gating strategy for CD24$^+$ cells and Siglec-10+ cells among PBMC cell types; after debris and doublet removal, monocytes were assessed as DAPI$^-$CD3$^-$CD14$^+$; T cells were assessed as DAPI$^-$CD14$^-$CD3$^+$; NK cells were assessed as DAPI$^-$CD14$^-$CD3$^-$CD56$^+$; B cells were assessed as DAPI$^-$ CD56$^-$CD14$^-$CD3$^-$CD19$^+$. Plots are representative of 2 experimental replicates. **d,** Frequency of PBMC cell types positive for Siglec-10 (blue shaded bars) or CD24 (red shaded bars) out of total cell type ($n = 3$ donors). **e,** (left) Flow cytometry–based measurement of the surface expression of Siglec-10 on primary human donor-derived macrophages either unstimulated (top) or following stimulation with M2-polarizing cytokines TGFβ1 and IL-10 (bottom), numbers above bracketed line indicate percent CD11b+ macrophages positive for expression of Siglec-10; (right) Frequency of primary human donor-derived macrophages positive for Siglec-10 either without stimulation (Unstimulated, M0) or following stimulation with TGFβ1 and IL-10 (Stimulated, M2-like), ($n = 30$ Unstimulated donors, 33 Stimulated donors; unpaired, two-tailed Student's t-test, ****P<0.0001, data are mean ±s.e.m.). **f,** Flow cytometry–based measurement of phagocytosis of MCF-7 cells by unstimulated donor-derived macrophages (white dots) versus TGFβ–1 and IL-10-stimulated donor-derived macrophages ($n = 3$ donors, unpaired, one-tailed t-test, *$P = 0.0168$). **g,** (left) Flow cytometry–based measurement of the surface expression of Siglec-10 on matched, primary donor-derived macrophages either unstimulated (gray shaded curve), or following stimulation with TGFβ1 and IL-10 (blue line), or IL-4 (green line); (right) Frequency of matched, human donor-derived macrophages positive for Siglec-10 either without stimulation (Unstimulated, M0), or following stimulation with TGFβ1 and IL-10 (blue dots), or stimulated with IL-4 ($n = 4$ donors). Data are mean ±s.e.m.
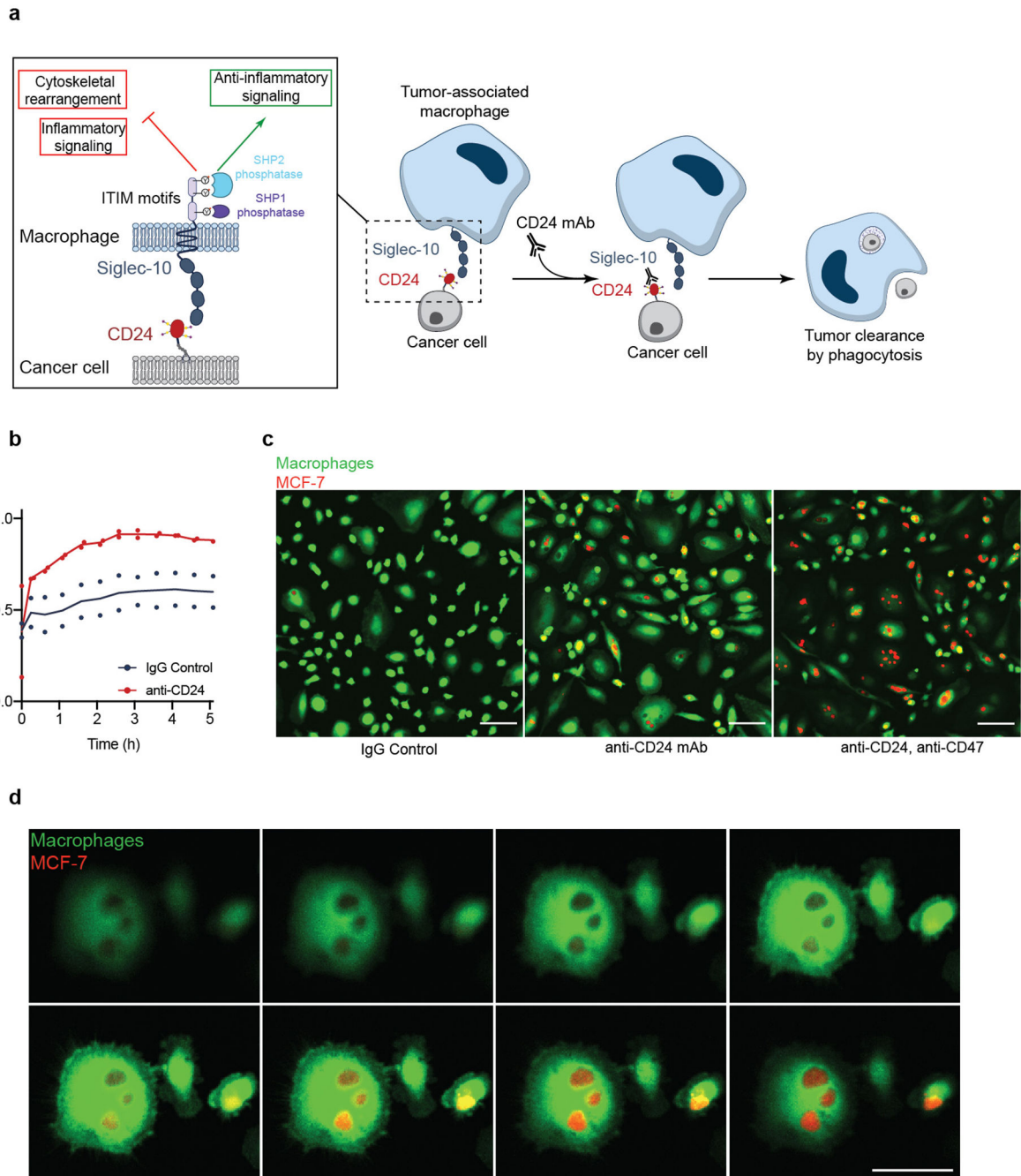
Extended Data Figure 3.

Siglec-10 binds to CD24 expressed on MCF-7 cells

a, Flow cytometry histogram measuring binding of Siglec-10 to WT MCF-7 cells (blue shaded curve) versus ΔCD24 MCF-7 cells (red shaded curve). Data are representative of two experimental replicates. **b,** Merged flow cytometry histogram measuring binding of Siglec-10-Fc to WT MCF-7 cells treated with heat-inactivated neuraminidase (WT-HI NA, blue line), WT MCF-7 cells treated with neuraminidase (WT-NA, green line), ΔCD24 MCF-7 cells treated with heat-inactivated neuraminidase (red line, ΔCD24-HI NA), and

ΔCD24 MCF-7 cells treated with neuraminidase (purple line, ΔCD24-NA) as compared to isotype control (black line). Data are representative of two experimental replicates. **c,** Flow cytometry–based measurement of phagocytosis of CD24^{+} parental MCF-7 cells (WT) and CD24^{−} (ΔCD24) MCF-7 cells by co-cultured human macrophages in the presence of neuraminidase (+NA) or heat-inactivated neuraminidase (+HI-NA) ($n = 4$ donors; two-way ANOVA with multiple comparison's correction, cell line $F_{(1,12)} = 180.5$, treatment $F_{(1,12)} = 71.12$, ****P<0.0001, data are mean ±s.e.m.). **f,h** Representative flow cytometry histogram measuring the binding of Siglec-5, **f**, or Siglec-9, **h**, to WT MCF-7 cells treated with either vehicle (blue shaded curve) or neuraminidase (green shaded curve). Data are representative of two experimental replicates. **g,i,** Frequency of macrophages positive for Siglec-5, **g**, or Siglec-9, **i**, among unstimulated M0 macrophages or stimulated M2-like macrophages ($n = 4$ donors). Data are mean ±s.e.m.

a,

b,

c,

d,

Extended Data Figure 4.

Anti-CD24 monoclonal antibodies promote phagocytic clearance of cancer cells over time

a, Schematic of CD24-Siglec-10 inhibition of phagocytosis; the inhibitory receptor Siglec-10 engages its ligand CD24 on cancer cells, leading to phosphorylation of the two ITIM motifs in the cytoplasmic domain of Siglec-10 and subsequent anti-inflammatory, anti-phagocytic signaling cascades mediated by SHP-1 and SHP-2 phosphatases; upon the addition of a CD24 blocking antibody, macrophages are disinhibited and thus capable of phagocytosis-mediated tumor clearance. **b,** Quantification of phagocytosis events (red[+]) of

MCF-7 cells treated with anti-CD24 mAb (red curve) versus IgG control (blue curve) as measured by live-cell microscopy over time in hours (h), normalized to maximum measured phagocytosis events per donor, (n = two donors; P value computed by two-way ANOVA of biological replicates, $F_{(1,24)} = 65.02$). Line is the mean of two biological replicates with individual replicates shown. **c,** Representative fluorescence microscopy images of *in vitro* phagocytosis of MCF-7 cells (mCherry$^+$, red) by macrophages (Calcein, AM; green) in the presence of IgG control (left), anti-CD24 mAb (middle), or anti-CD24 mAb and anti-CD47 mAb (right), after 6 hours of co-culture. Experiment was repeated with three donors. Scale bar represents 100 μm. **d,** Representative *Z*-stack images collected from high-resolution confocal fluorescence microscopy of macrophage phagocytosis demonstrating engulfment of whole MCF-7 cells (mCherry$^+$, red) by macrophages (Calcein, AM; green). Experiment was repeated with three donors. Scale bar represents 50 μm.

a, Gating strategy for *in vitro* phagocytosis
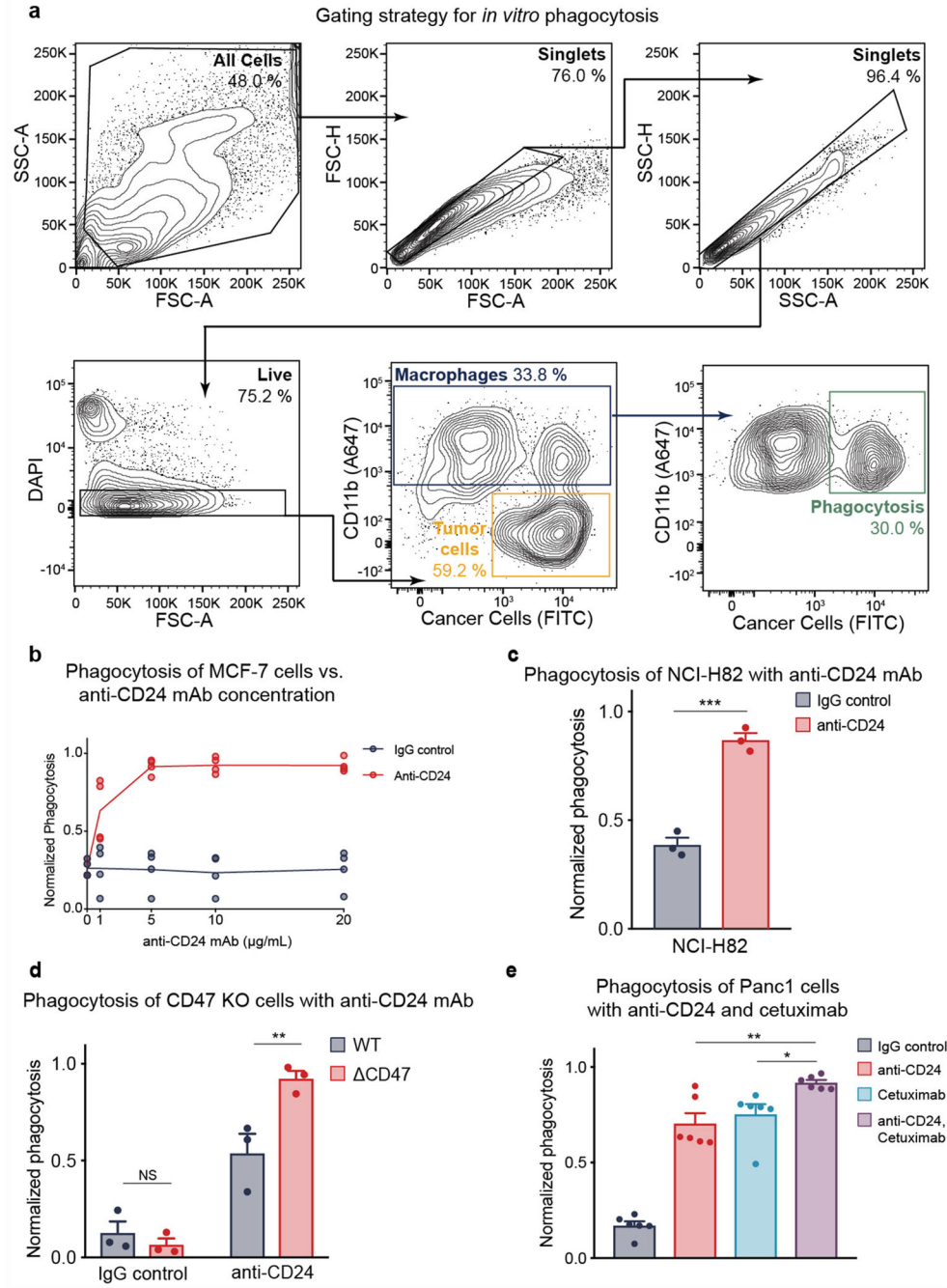
Extended Data Figure 5.

CD24 antibody blockade of CD24-Siglec-10 signaling promotes dose-responsive enhancement of phagocytosis

a, Gating strategy for *in vitro* phagocytosis assay. Following debris and doublet removal, phagocytosis was assessed as the frequency of DAPI⁻CD11b⁺FITC⁺ events out of all DAPI⁻CD11b⁺ events. Numbers indicate frequency of events out of previous gate. Plots are representative of at least 10 experimental replicates. **b,** Dose-response relationship of anti-CD24 mAb on phagocytosis of MCF-7 cells, concentrations listed on the x-axis as compared

to IgG control ($n = 3$ donors). Connecting line is mean. **c,** Flow cytometry–based measurement of phagocytosis of NCI-H82 cells by donor-derived macrophages ($n = 3$ donors) in the presence of anti-CD24 mAb as compared to IgG control; each symbol represents an individual donor (paired, two-tailed Student's *t*-test, ***$P = 0.0001$). Data are mean ±s.e.m. **d,** Flow cytometry–based measurement of phagocytosis of CD24$^+$ parental MCF-7 cells (WT) and CD47$^-$ (ΔCD47) MCF-7 cells by co-cultured human macrophages, in the presence or absence of anti-CD24 mAb (horizontal axis), ($n = 4$ donors; two-way ANOVA with multiple comparisons correction, cell line $F_{(1,8)} = 6.490$; treatment $F_{(1,8)} = 98.73$, **$P = 0.0054$). Data are mean ±s.e.m. **e,** Flow cytometry –based measurement of phagocytosis of Panc1 pancreatic adenocarcinoma cells in the presence of anti-CD24 mAb, cetuximab (anti-EGFR), or both anti-CD24 mAb and cetuximab, as compared to IgG control ($n = 6$ donors) (one-way ANOVA with multiple comparisons correction, $F_{(3,20)} = 66.10$. *$P = 0.0373$, **$P = 0.0057$. Data are mean ±s.e.m.
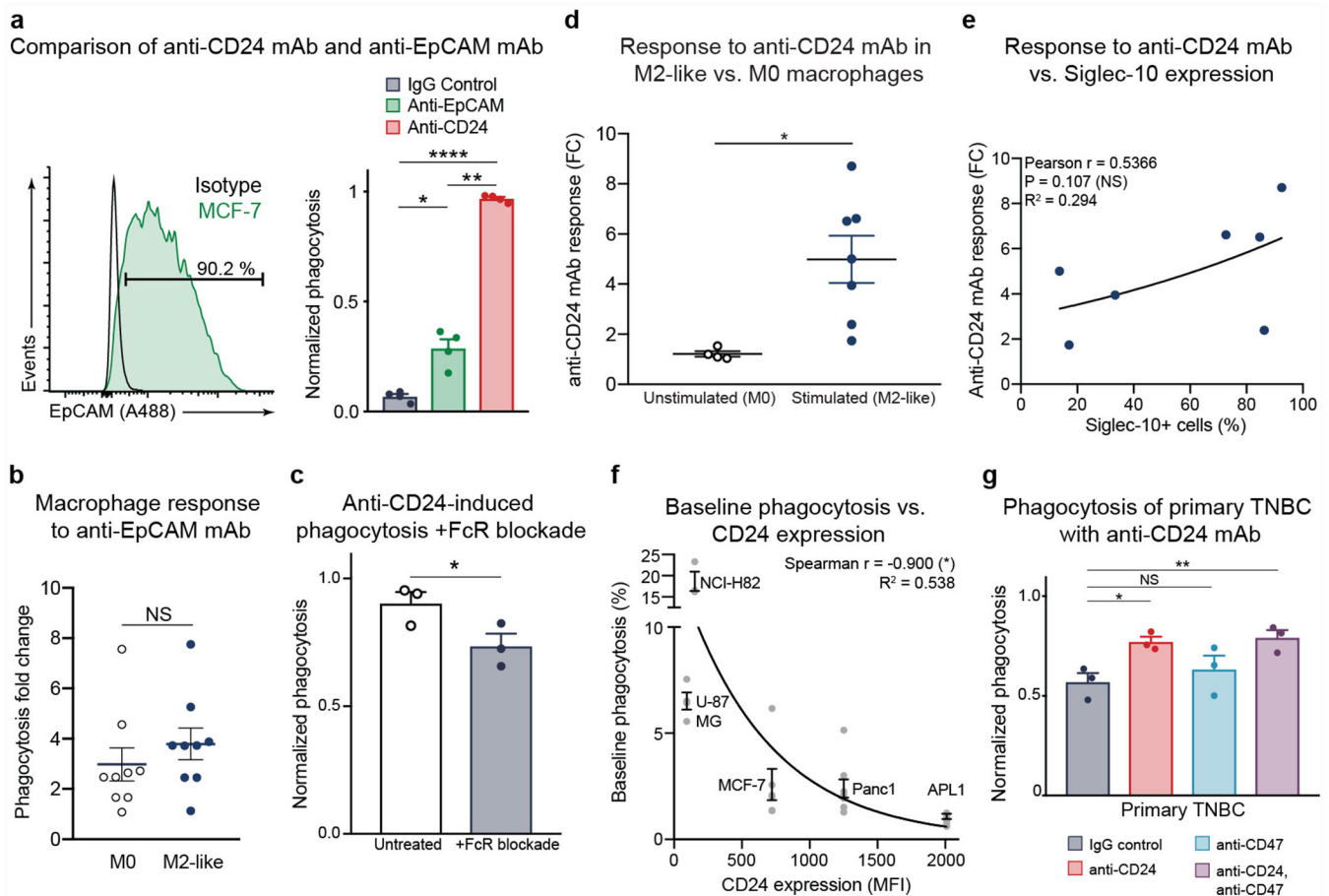
a, (left) Representative flow cytometry histogram measuring the expression of EpCAM (green shaded curve) by parental MCF-7 cells, number above bracketed line indicates percent MCF-7 cells positive for expression of EpCAM; (right) Flow cytometry–based measurement of phagocytosis of parental MCF-7 cells by co-cultured human macrophages, in the presence of either IgG control, anti-EpCAM mAb, or anti-CD24 mAb ($n = 4$ donors; repeated measures ANOVA with multiple comparisons correction, $F_{(2,9)} = 340.9$, $*P = 0.0287$, $**P = 0.0015$, $****P < 0.0001$). Data are mean ±s.e.m. **b,** Fold change in phagocytosis by M0 (unstimulated) or M2-like (TGFβ–1, IL-10-stimulated) macrophages upon the addition of anti-EpCAM mAb as compared to IgG control, ($n = 9$ donors. Paired, two-tailed t-test, NS = not significant). Data are mean ±s.e.m. **c,** Flow cytometry–based measurement of anti-CD24 mAb-induced phagocytosis of MCF-7 cells by untreated macrophages (white bar) versus macrophages treated with anti-CD16/32 mAb (+FcR blockade, blue bar) ($n = 3$ macrophage donors. Paired, two-tailed t-test. Each point represents an individual donor. $*P = 0.0358$). Data are mean ±s.e.m. **d,** Response to anti-CD24 mAb by M2-like macrophages vs. M0 macrophages; each symbol represents an individual donor ($n = 4$ M0 donors, $n = 6$ M2-like donors; unpaired, two-tailed Student's t-test, $*P = 0.0160$). **e,** Pearson correlation between stimulated (M2-like) donor-derived

macrophage Siglec-10 expression (MFI = median fluorescence intensity) (x-axis) and response to anti-CD24 mAb as computed by the phagocytosis fold change between anti-CD24 mAb treatment and IgG control (y-axis), (n = 7 donors); exponential growth curve is shown. **f,** Spearman correlation between cancer cell CD24 expression (MFI = median fluorescence intensity) (x-axis) and baseline, un-normalized phagocytosis levels (IgG control) averaged across all donors per cell line. Exponential growth equation is shown. (n are same as in Figure 3b and Extended Data Figure 5c, *P = 0.0417). Data are mean ±s.e.m. **g,** Flow cytometry–based measurement of phagocytosis of a patient sample of primary TNBC cells in the presence of anti-CD24 mAb, anti-CD47 mAb, or both anti-CD24 mAb and anti-CD47 mAb, as compared to IgG control (n = 3 macrophage donors challenged with n = 1 primary TNBC donor. Repeated measures one-way ANOVA with multiple comparisons correction, $F_{(1.217, 2.434)}$ = 26.17). Each point represents an individual donor. NS = not significant, *P = 0.0434, **P = 0.0028. Data are mean ±s.e.m.

Gating strategy for *in vivo* phagocytosis
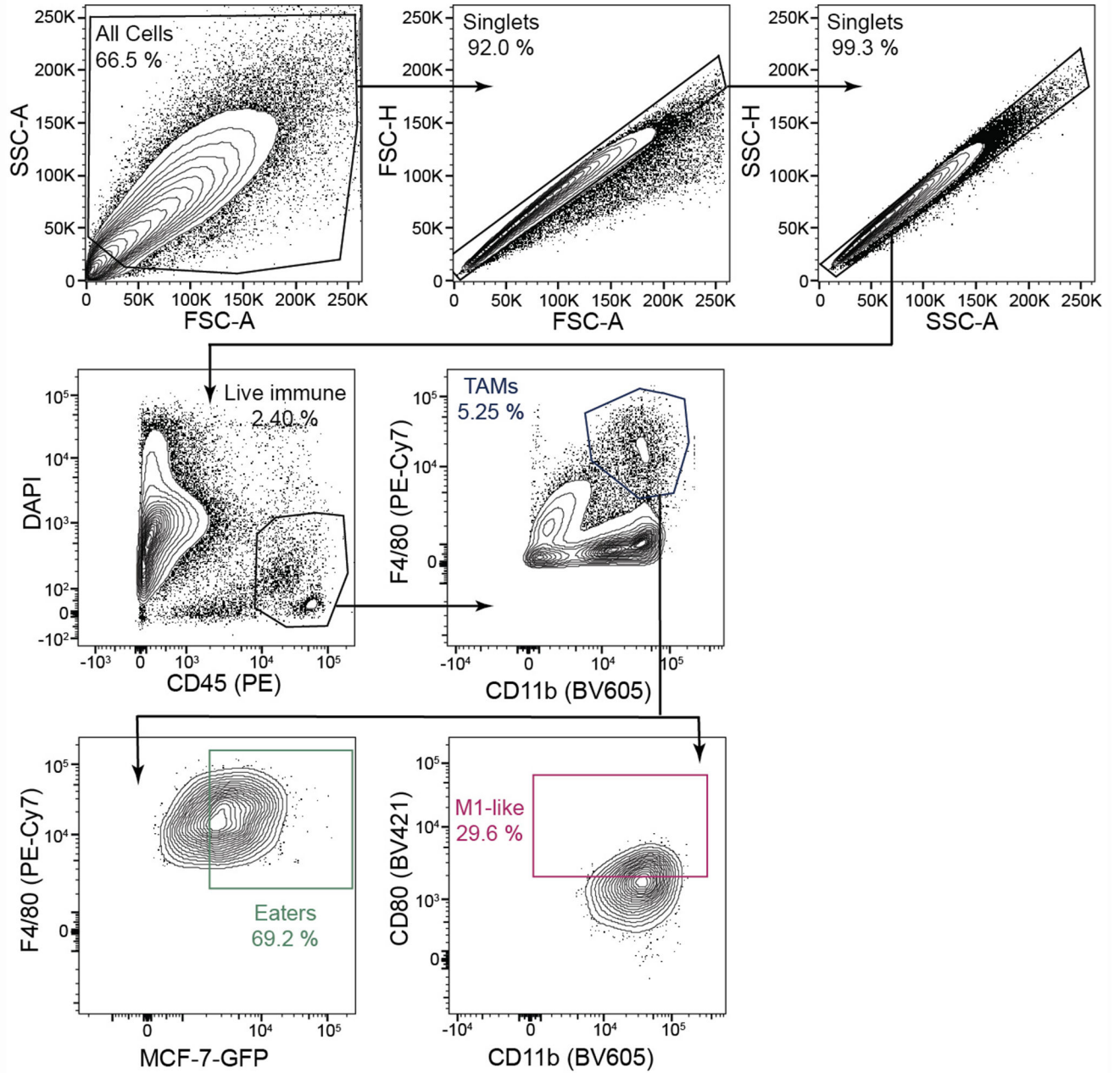
Extended Data Figure 7.

Gating strategy for *in vivo* phagocytosis

Gating strategy for *in vivo* TAM phagocytosis of MCF-7 cells; following debris and doublet removal, TAM phagocytosis assessed as the frequency of DAPI⁻CD11b⁺F4/80⁺GFP⁺ events out of total DAPI⁻CD11b⁺F4/80⁺ events; M1-like TAMs assessed as DAPI⁻CD11b⁺F4/80⁺CD80⁺, Numbers indicate frequency of events out of previous gate. Plots are representative of three experimental replicates.
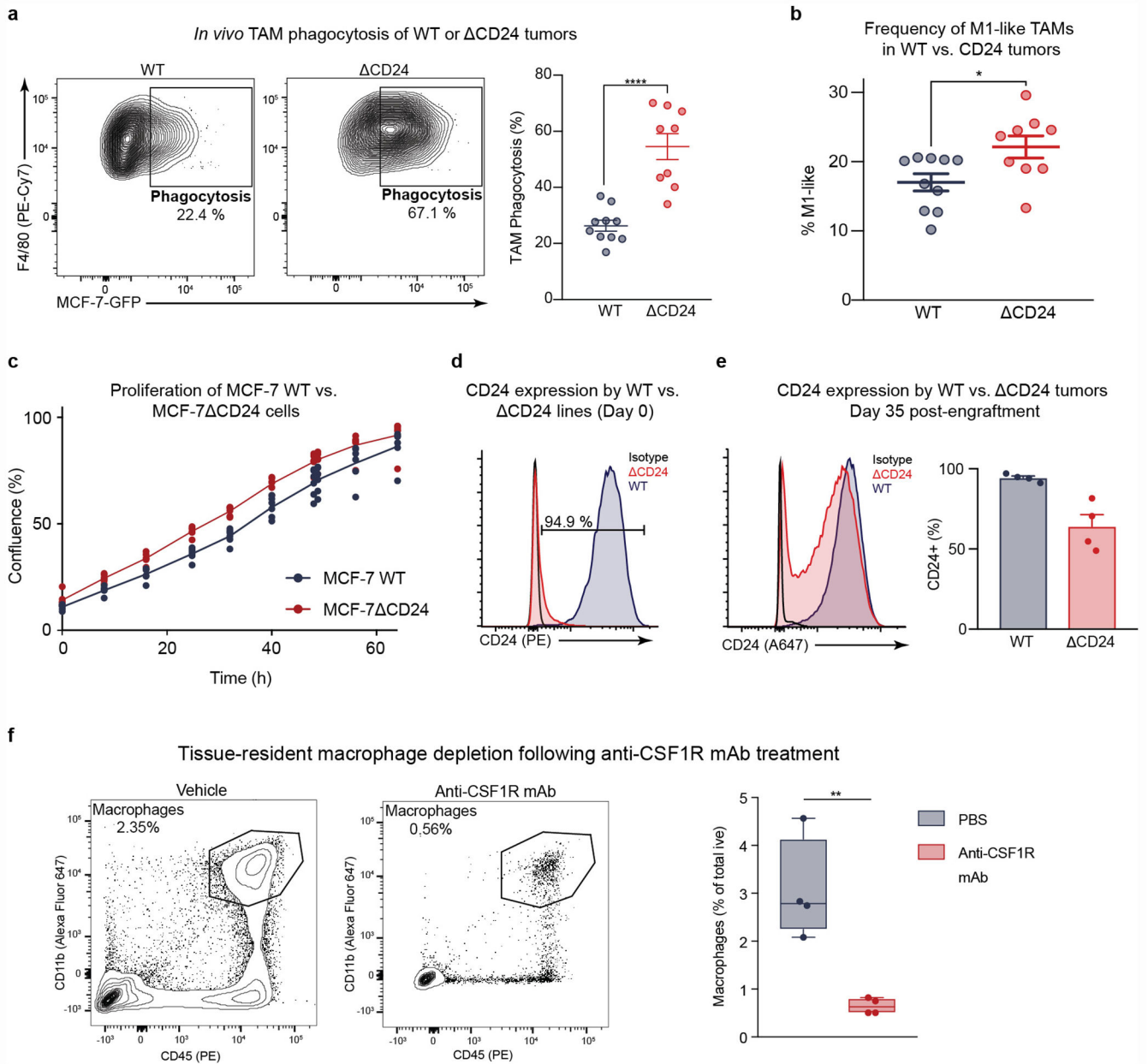
Extended Data Figure 8.

Characterization of MCF-7 WT and MCF-7 CD24 cells *in vitro* and *in vivo*

a, Representative flow cytometry plots demonstrating TAM phagocytosis in GFP-luciferase^{+} CD24^{+} (WT) MCF-7 tumors (left) vs. CD24^{−} (CD24) MCF-7 tumors (middle), numbers indicate frequency of phagocytosis events out of all TAMs; (right) frequency of phagocytosis events out of all TAMs in WT tumors vs. CD24 tumors 28 days after engraftment (WT $n =$ 10, CD24 $n = 9$. Unpaired, two-tailed Student's *t*-test, ****P<0.0001). **b,** Frequency of TAMs positive for CD80 (M1-like) as per gating in **a,** among all TAMs macrophages as defined by fluorescence minus one controls (WT $n = 10$, CD24 $n = 9$. Unpaired, two-tailed Student's *t*-test, *P<0.0203). Data are mean ±s.e.m. **c,** *In vitro* proliferation rates of MCF-7 WT and MCF-7 CD24 as assessed by confluence percentage (y-axis) over time (x-axis), (*n*

= 6 technical replicates, one experimental replicate) Individual technical replicates shown, connecting line indicates mean. **d,** Flow cytometry-based measurement of the surface expression of CD24 on MCF-7 cells (blue shaded curve) versus CD24 knockout cells (ΔCD24) (red shaded curve) prior to tumor engraftment as compared to isotype control (black line), numbers above bracketed line indicate percent MCF-7 WT cells positive for expression of CD24. Plot is representative of 10 experimental replicates. **e,** (left) Representative flow cytometry histogram of the surface expression of CD24 on Day 35 WT MCF-7 tumors (blue shaded curve) versus Day 35 CD24 knockout tumors (ΔCD24) (red shaded curve) as compared to isotype control (black line); (right) flow cytometry–based measurement of the frequency of $CD24^+$ cells among all cancer cells in Day 35 WT tumors versus Day 35 ΔCD24 tumors (WT $n = 4$, ΔCD24 $n = 4$). Data are mean ±s.e.m. **f,** Representative flow cytometry plots of tissue-resident macrophages out of total live cells in vehicle-treated animals (left) vs. anti-CSF1R-treated animals (middle), numbers indicate frequency of CD11b+,F4/80+ macrophage events out of total live events; (right) frequency of TAMs (CD11b+,F4/80+) out of total live cells in vehicle-treated animals ($n = 5$, blue shaded boxplot) vs. anti-CSF1R-treated animals ($n = 4$, red shaded boxplot) as measured by flow cytometry. **P<0.01. Boxplots depict mean and range.
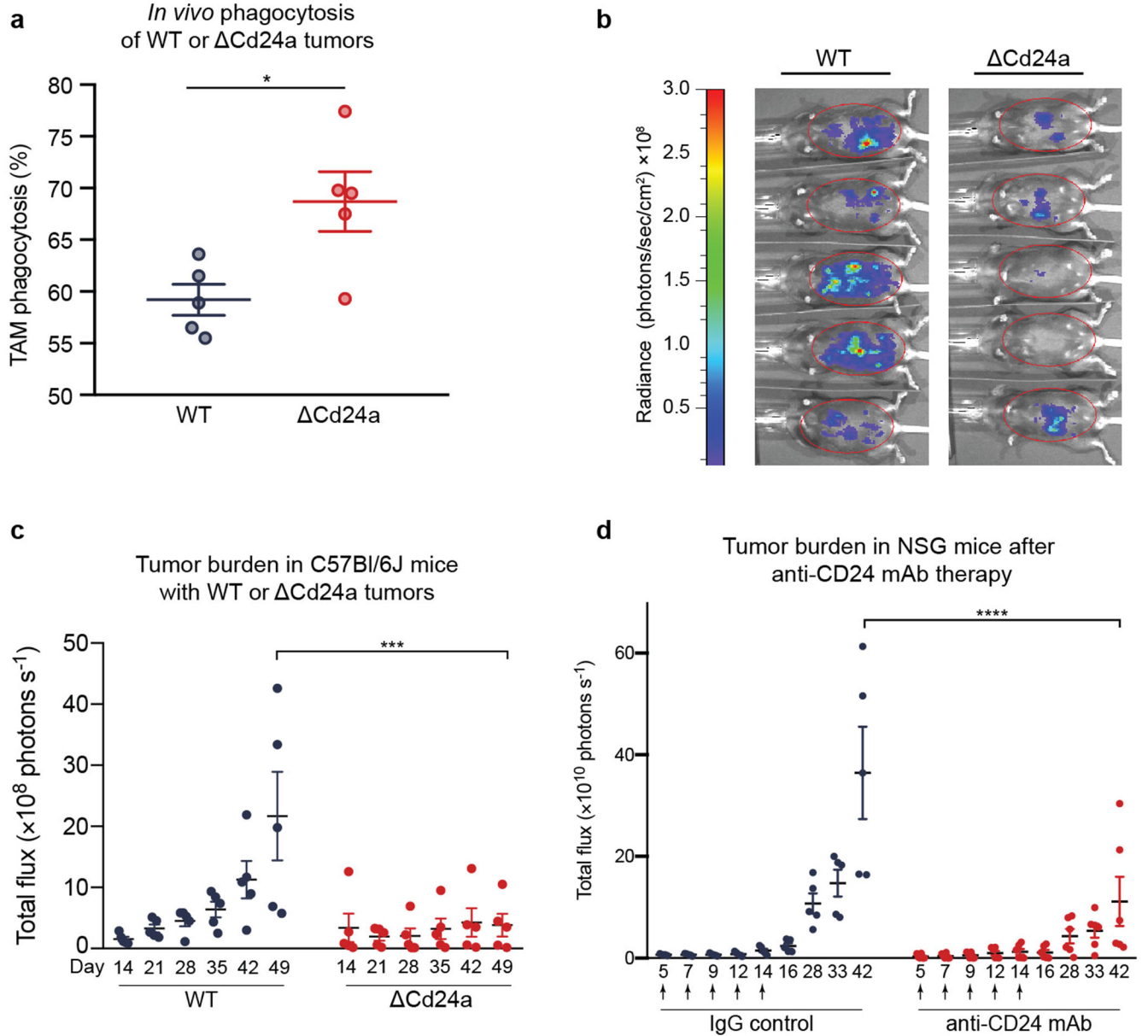
Extended Data Figure 9.

Validation of CD24 inhibition in *in vivo* models of ovarian and breast cancer

a, *In vivo* phagocytosis of WT or ΔCd24a cancer cells by mouse TAMs Flow cytometry–based measurement of *in vivo* phagocytosis of CD24+GFP+ ID8 cells (WT) versus CD24−GFP+ ID8 cells (ΔCd24a) by mouse peritoneal macrophages, ($n = 5$ mice; unpaired, two-tailed Student's *t*-test with multiple comparisons correction, *$P = 0.0196$). **b,** Representative bioluminescence image of tumor burden in C57Bl/6 mice with ID8 WT vs. ID8 ΔCd24a tumors (image taken 49 days post-engraftment and representative of one experimental replicate). **c,** Burden of ID8 WT tumors (blue) vs. ID8 ΔCd24a tumors (red) as measured by bioluminescence imaging (WT $n = 5$, ΔCd24a $n = 5$. Two-way ANOVA with multiple comparisons correction, tumor genotype $F_{(1,48)} = 10.70$, ***$P = 0.0001$). Data are
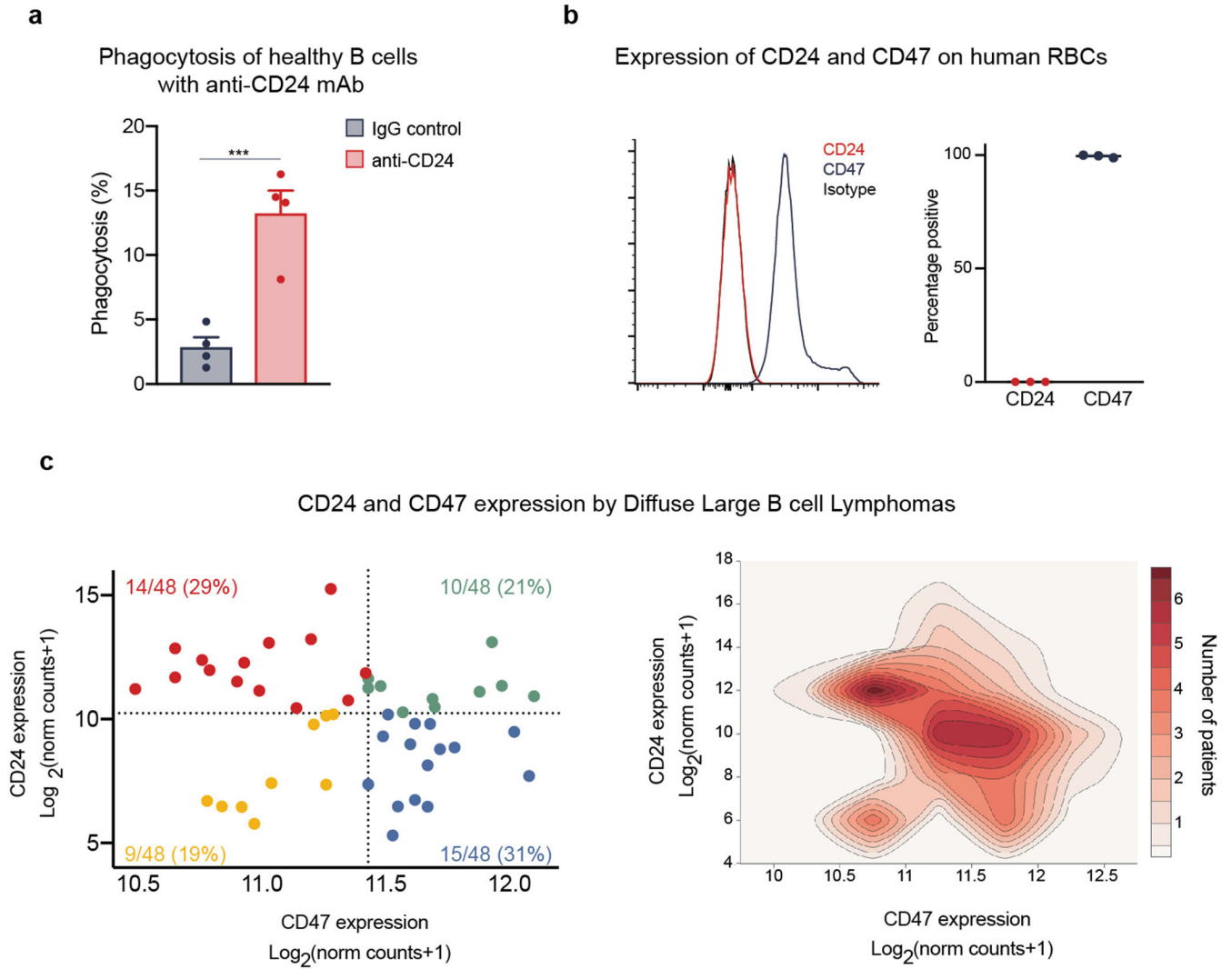
representative of one experimental replicate. **d,** Extended measurement (as in Figure 4e) of burden of MCF-7 WT tumors treated with IgG control (blue) vs. anti-CD24 mAb (red) as measured by bioluminescence (IgG control $n = 5$, anti-CD24 mAb $n = 5$. Days on which anti-CD24 mAb was administered are indicated by arrows below x-axis. Data are of one independent experimental cohort. Two-way ANOVA with multiple comparisons correction, tumor treatment $F_{(1,81)} = 16.75$). ****$P<0.0001$. Data are mean ±s.e.m.

a

Phagocytosis of healthy B cells
with anti-CD24 mAb

b

Expression of CD24 and CD47 on human RBCs

c

CD24 and CD47 expression by Diffuse Large B cell Lymphomas

Extended Data Figure 10.

Anti-CD24 mAb induces B cell clearance but does not bind human RBCs, and CD47 and CD24 subset human DLBCL demonstrating inversely correlated expression

a, Flow cytometry–based measurement of phagocytosis of B cells ($n = 4$ donors, pooled) by donor-derived macrophages ($n = 4$ donors) in the presence of anti-CD24 mAb as compared to IgG control; each symbol represents an individual donor (paired, two-tailed Student's t-test, ***$P = 0.0008$). **b,** (left) Representative flow cytometry histogram measuring the expression of CD24 (red line) and CD47 (blue line) by human RBCs; (right) Flow-cytometry–based measurement of the frequency of CD24+ versus CD47+ RBCs out of total RBCs ($n = 3$ donors). Data are mean ±s.e.m. **c,** (left) Expression levels in $\log_2$(norm counts + 1) of CD24 and CD47 in Diffuse Large B Cell Lymphomas from TCGA ($n = 48$), data are divided into quadrants by median expression of each gene as indicated by dotted lines, number and percentage of total patients in each quadrant indicated on plot. Each dot indicates a single patient; (right) 2-dimensional contour plot of Diffuse Large B Cell Lymphoma patients in left plot.

Supplementary Material

Refer to Web version on PubMed Central for supplementary material.

Acknowledgements:

References:

1. Majeti R et al. CD47 is an adverse prognostic factor and therapeutic antibody target on human acute myeloid leukemia stem cells. Cell **138:** Cell 138, 286–299 (2009) [PubMed: 19632179]

2. Gordon SG et al. PD-1 expression by tumour-associated macrophages inhibits phagocytosis and tumour immunity. Nature 545, 495–499 (2017) [PubMed: 28514441]

3. Barkal AA et al. Engagement of MHC class I by the inhibitory receptor LILRB1 suppresses macrophages and is a target of cancer immunotherapy. Nature Immunology 19, 76–84 (2018) [PubMed: 29180808]

4. Advani R et al. CD47 blockade by Hu5F9-G4 and rituximab in non-Hodgkin's lymphoma. New England Journal of Medicine 379, 1711–1721

5. Willingham SB et al. The CD47-SIRPa interaction is a therapeutic target for human solid tumors. Proc. Natl. Acad. Sci. USA 109, 6662–6667 (2012). [PubMed: 22451913]

6. Pirruccello SJ, LeBien TW The human B cell-associated antigen CD24 is a single chain sialoglycoprotein. J. Immunol. 136, 3779–3784 (1986). [PubMed: 2939133]

7. Chen GY, Brown NK, Zheng P, Liu Y Siglec-G/10 in self-nonself discrimination of innate and adaptive immunity. Glycobiology 9, 800–806 (2014).

8. Chen W et al. Induction of Siglec-G by RNA viruses inhibits the innate immune response by promoting RIG-I degradation. Cell 152(3), 467–478. [PubMed: 23374343]

9. Chen GY et al. Amelioration of sepsis by inhibiting sialidase-mediated disruption of the CD24-SiglecG interaction. Nature Biotechnology 29, 428–435 (2011)

10. Chen GY et al. CD24 and Siglec-10 selectively repress tissue damage-induced immune responses. Science 323 (5922), 1722–1725 (2009) [PubMed: 19264983]

11. Toubai T et al. Siglec-G-CD24 axis controls the severity of graft-versus-host disease in mice. Blood 123(22), 3512–3513 (2014) [PubMed: 24695850]

12. Crocker PR, Paulson JC, Varki A Siglecs and their roles in the immune system. Nature Reviews Immunology. 7, 255–266 (2007)

13. Abram CL, Lowell CA Shp1 function in myeloid cells. J. Leuko.c Biol. 102(3), 657–675 (2017)

14. Dietrich J, Cella M, Colonna M Ig-Like Transcript 2 (ILT2)/Leukocyte Ig-Like Receptor 1 (LIR1) Inhibits TCR Signalling and Actin Cytoskeleton Reorganization. J. Immunol. 166(4), 2514–2521 (2001) [PubMed: 11160312]

15. Tarhriz V et al. Overview of CD24 as a new molecular marker in ovarian cancer. J. Cell. Physiol. 234(3) 2134–2142 (2019) [PubMed: 30317611]

16. Kristiansen G et al. CD24 expression is a new prognostic marker in breast cancer. Clin. Cancer. Res. 15(9), 4906–4913 (2003).

17. Karaayvaz M et al. Unravelling subclonal heterogeneity and aggressive disease states in TNBC through single-cell RNA-seq. Nature Communications 9, 3588 (2018)

18. Mantovani A, Sozzani S, Locati M, Allavena P, Sica A Macrophage polarization: tumor-associated macrophages as a paradigm for polarized M2 mononuclear phagocytes. Trends in Immunology 23(11), 549–555 (2002) [PubMed: 12401408]

19. Liu J et al. Pre-clinical development of a humanized anti-CD47 antibody with anti-cancer therapeutic potential. PLoS One 10, e0137345 (2015) [PubMed: 26390038]

20. Miksa M, Komura H, Wu R, Shah KG, Wang P A novel method to determine the engulfment of apoptotic cells by macrophages using pHrodo succinimidyl ester. J. Immunol. Methods 342(1-2), 71–77 (2009) [PubMed: 19135446]

21. Okazaki M, Luo Yi., Han Tin., Yoshida M, Seon BK Three New Monoclonal Antibodies That Define a Unique Antigen Associated With Prolymphocytic Leukemia/Non-Hodgkin's Lymphoma and Are Effectively Internalized After Binding to the Cell Surface Antigen. Blood 81 (1), 84–94 (1993) [PubMed: 8417805]

22. Shultz LD et al. Human lymphoid and myeloid cell development in NOD/LtSz-scid IL2Rγ null mice engrafted with mobilized human hemopoietic stem cells. J. Immunol. 174, 6477–6489 (2005) [PubMed: 15879151]

23. Varga A et al. Pembrolizumab in patients (pts) with PD-L1–positive (PD-L1+) advanced ovarian cancer: updated analysis of KEYNOTE-028. J. Clin. Oncol. 35 (abstract 5513) (2017)

24. Nanda R et al. Pebrolizumab in patients with advanced triple-negative breast cancer: Phase Ib KEYNOTE-012 study. J. Clin. Oncol. 34, 2460–2467 (2016) [PubMed: 27138582]

25. Alsaab HO et al. PD-1 and PD-L1 Checkpoint Signaling Inhibition for Cancer Immunotherapy: Mechanism, Combinations, and Clinical Outcome. Frontiers in Pharmacology 8, 561 (2017) [PubMed: 28878676]

26. Ayers M et al. Molecular Profiling of Cohorts of Tumor Samples to Guide Clinical Development of Pembrolizumab as Monotherapy. Clinical Cancer Res (2018)

27. Goldman M, Craft B, Brooks AN, Zhu J, Haussler D The USCS Xena Platform for cancer genomics data visualization and interpretation. bioRxiv. (2018)

28. Martinez FO Analysis of Gene Expression and Gene Silencing in Human Macrophages. Current Protocols in Immunology. 96(1), 14.28.1–14.28.23 (2012)

29. Brinkman EK et al. Easy quantitative assessment of genome editing by sequence trace decomposition. Nucleic Acids Research. 42(22), e168 (2014) [PubMed: 25300484]
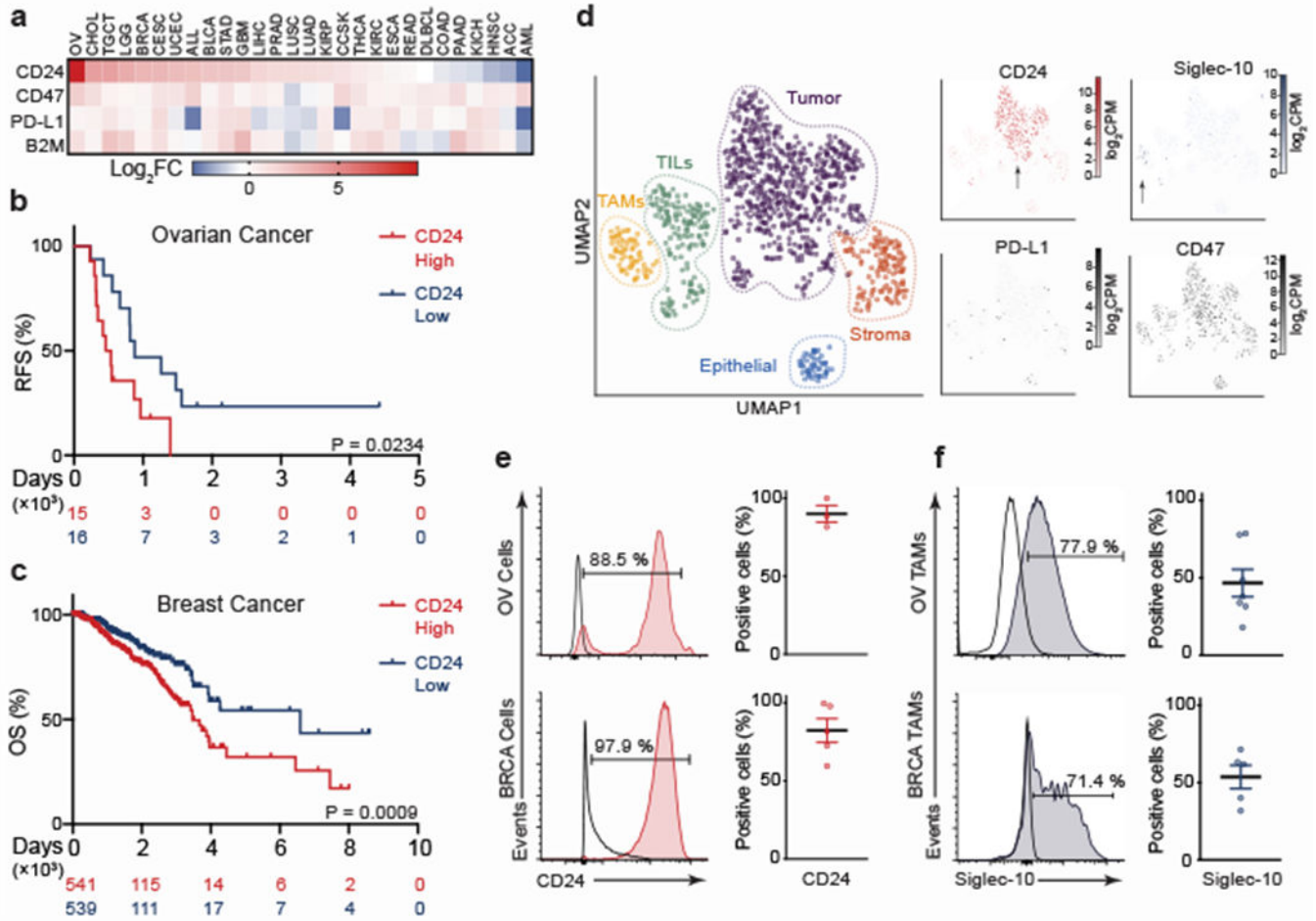
Figure 1.

CD24 is over-expressed by human cancers and is co-expressed with Siglec-10 on TAMs
a, Heatmap of CD24 tumor to matched normal expression ratios (log$_2$FC) compared to known immune checkpoints (tumor study abbreviations and n defined in Supplementary Table 1). **b,c,** Relapse-free survival percentage (RFS) for ovarian cancer patients ($n = 31$), **b,** and overall survival percentage (OS) for breast cancer patients ($n = 1080$), **c,** with high versus low CD24 expression as defined by median. Two-sided P value computed by a log-rank (Mantel-Cox) test. Numbers of subjects at risk in high group (red) vs. low group (blue) indicated below the x-axes. **d,** UMAP dimension 1 and 2 plots displaying TNBC cells from 6 patients ($n = 1001$ single cells); (left) cells colored by cluster identity, (right) CD24 (red) and Siglec-10 (blue) expression overlaid onto UMAP space as compared to CD47 (gray) and PD-L1 expression (gray). **e,** (left) Representative flow cytometry histogram of CD24 expression by ovarian cancer (OV) cells (top) or breast cancer (BRCA) cells (bottom); (right) frequency of CD24$^+$ cancer cells in ovarian cancer ($n = 3$ donors) (top) or breast cancer ($n = 5$ donors) (bottom). Data are mean ±s.e.m. **f,** (left) Representative flow cytometry histogram measuring the expression of Siglec-10 by ovarian cancer (OV) TAMs (top) or breast cancer (BRCA) TAMs (bottom); (right) frequency of Siglec-10$^+$ TAMs in ovarian cancer ($n = 6$ donors) (top) or breast cancer ($n = 5$ donors) (bottom). Data are mean ±s.e.m.
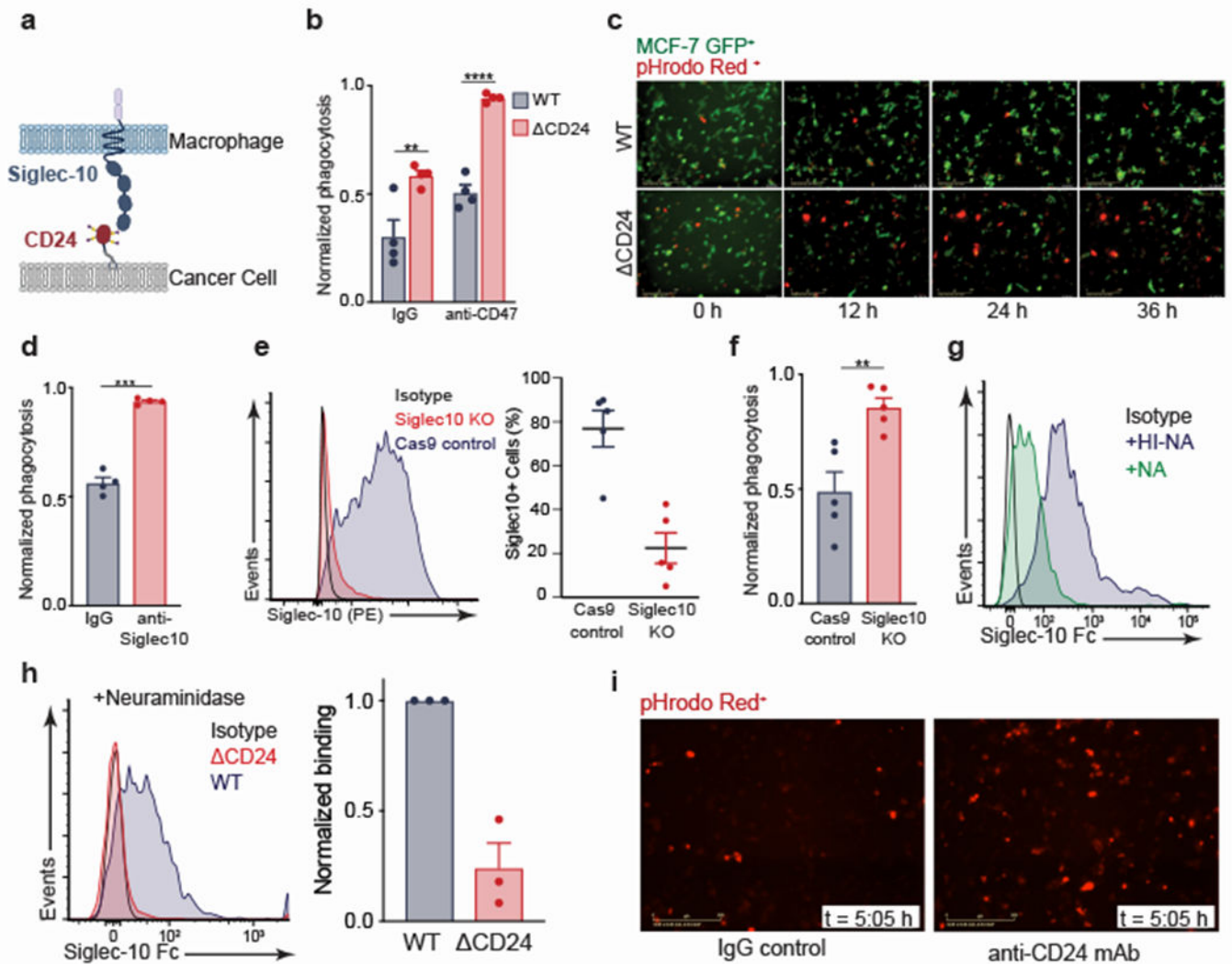
Figure 2.
CD24 directly protects cancer cells from phagocytosis by macrophages

a, Schematic depicting interactions between macrophage-expressed Siglec-10 and CD24 expressed by cancer cells. **b,** Phagocytosis of CD24$^+$ MCF-7 cells (WT) and CD24$^-$ (ΔCD24) MCF-7 cells, in the presence or absence of anti-CD47 mAb, ($n = 4$ donors; two-way ANOVA with multiple comparisons correction, cell line $F_{(1,12)} = 65.65$; treatment $F_{(1,12)} = 40.30$, **$P = 0.0045$, ****$P<0.0001$). **c,** Representative phagocytosis images of pHrodo-red$^+$, GFP$^+$ MCF-7 cells (WT, top; ΔCD24, bottom) over time (hours); images representative of two donors. **d,** Phagocytosis of WT MCF-7 cells, in the presence of anti-Siglec-10 mAb or IgG control ($n = 4$ donors; paired, two-tailed Student's t-test, ***$P = 0.0010$). **e,** (left) FACS–based measurement of Siglec-10 expression by Siglec-10 KO macrophages (red) vs. Cas9 control (blue); (right) Frequency of Siglec-10$^+$ macrophages among Cas9 control vs. Siglec-10 KO macrophages. Data are mean±s.e.m of $n = 5$ donors. **f,** Phagocytosis of WT MCF-7 cells by either Siglec-10 KO or Cas9 control macrophages. Data are mean±s.e.m of $n = 5$ donors; paired, one-tailed Student's t-test, **$P = 0.0035$. **g,** Flow cytometry–based measurement of binding of recombinant Siglec-10-Fc to MCF-7 WT

cells treated with neuraminidase (+NA) or heat-inactived neuraminidase (+HI-NA); plot is representative of two experimental replicates. **h,** (left) Flow cytometry–based measurement of binding of Siglec-10-Fc to neuraminidase-treated MCF-7 WT cells vs. neuraminidase-treated MCF-7 CD24 cells. Plot is representative of 3 experimental replicates; (right) normalized binding of Siglec-10-Fc to neuraminidase-treated MCF7 CD24 cells vs. neuraminidase-treated MCF7 WT cells. Data are representative of 3 experimental replicates. **i,** Representative images from live-cell microscopy phagocytosis assays of pHrodo-red[+] MCF-7 cells treated with anti-CD24 mAb (right) or IgG control (left) at $t = 5:05$ h; images are representative of two donors and two experimental replicates.
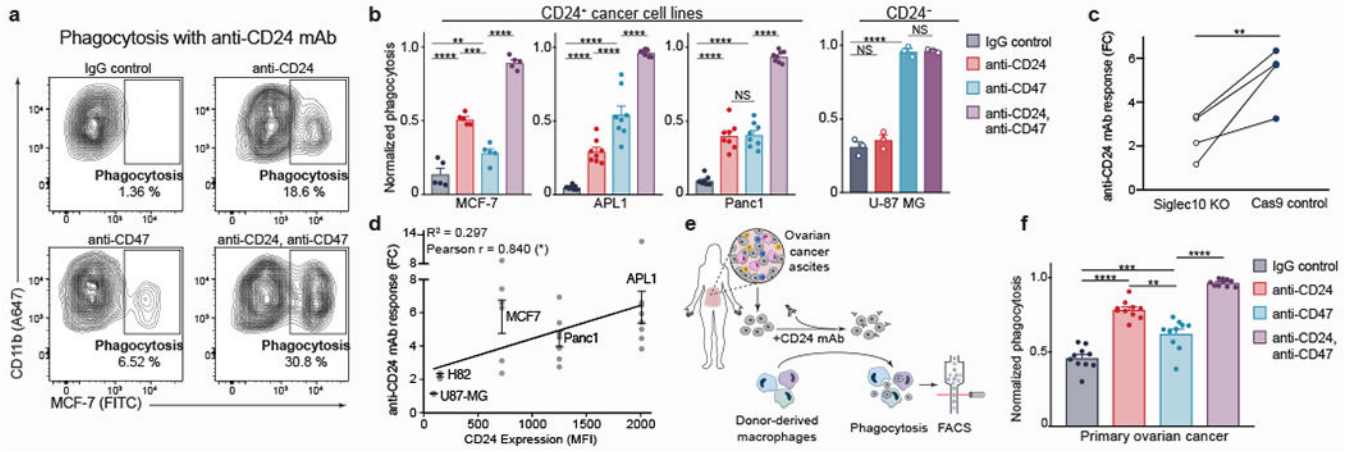
Figure 3.

Treatment with anti-CD24 mAb promotes phagocytic clearance of human cancer cells

a, Representative flow cytometry plots depicting phagocytosis of MCF-7 cells treated with anti-CD24 mAb, CD47 mAb, or dual treatment vs. IgG control. Plots representative of 5 donors. **b,** Phagocytosis of MCF-7 ($n = 5$ donors), APL1 ($n = 8$ donors), and Panc1 ($n = 8$ donors) (left) and U87-GM cell line ($n = 3$ donors; solid bars) (right) in the presence of anti-CD24 mAb, anti-CD47 mAb or dual treatment vs. IgG control (one-way ANOVA with multiple comparisons correction; MCF-7 $F_{(3,16)} = 145.6$, APL1 $F_{(3,28)} = 144.7$, Panc1 $F_{(3,28)} = 220.7$, U-87 MG $F_{(3,8)} = 200.4$; NS = not significant, $**P = 0.0092$, $***P = 0.0001$, $****P < 0.0001$). **c,** Response to anti-CD24 mAb by Siglec-10 KO vs. Cas9 control macrophages ($n = 4$ donors, connecting lines indicate matched donor. Paired, one-tailed Student's t-test, $**P = 0.0089$) **d,** Pearson correlation between CD24 expression (x-axis) and mean anti-CD24 mAb response (y-axis) (n are same as listed in **b,** and Extended Data Figure 5c. Linear regression is shown. Error bars are mean ±s.e.m. $*P = 0.0375$). **e,** Workflow to measure phagocytosis of primary ovarian cancer, **f,** Phagocytosis of primary ovarian cancer cells treated with anti-CD24 mAb, anti-CD47 mAb, or dual treatment vs. IgG control ($n = 10$ macrophage donors, $n = 1$ primary ovarian cancer ascites donor) (one-way ANOVA with multiple comparisons correction, $F_{(2.110, 18.99)} = 121.5$, $**P = 0.0078$, $***P = 0.0006$, $****P < 0.0001$). Data are mean ±s.e.m.
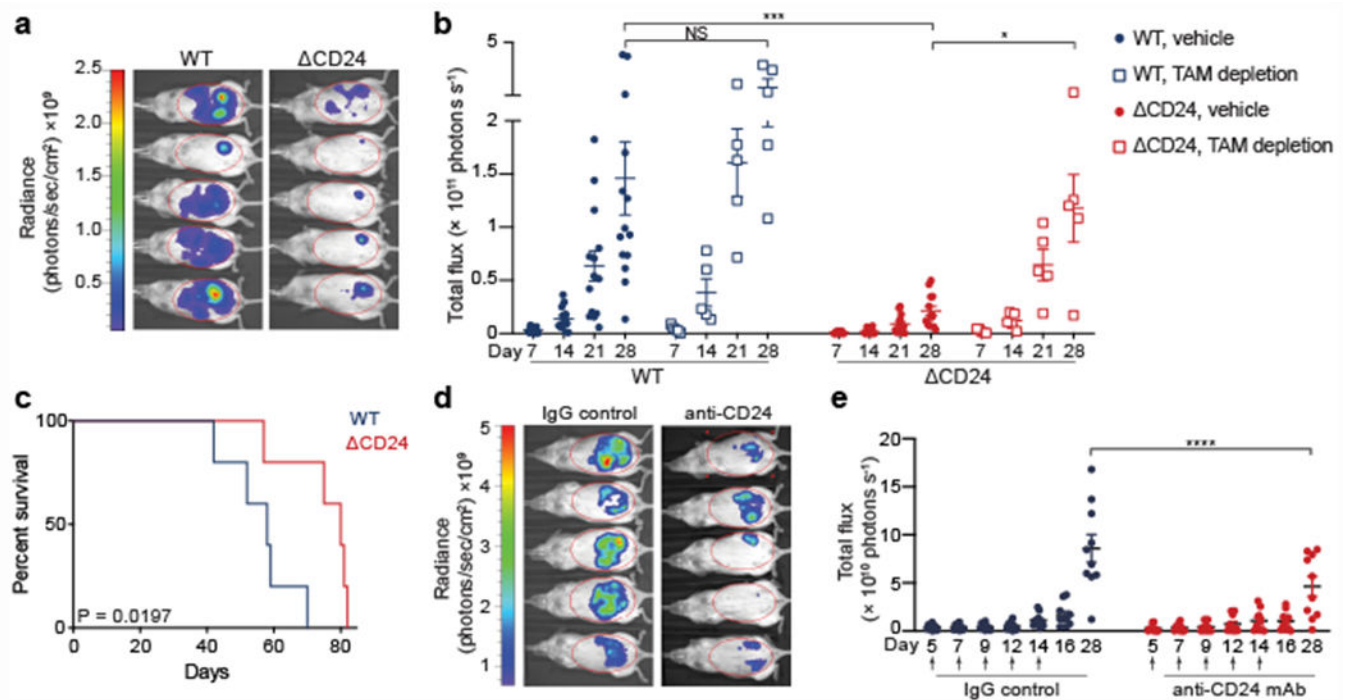
Figure 4.

CD24 protects cancer cells from macrophage attack *in vivo*

a, Representative bioluminescence image of Day 21 tumors in mice engrafted with MCF-7 WT vs. MCF-7 ΔCD24 tumors (image representative of two independent experimental cohorts). **b,** Burden of MCF-7 WT vs. MCF-7 ΔCD24 tumors in mice with TAMs (vehicle) or TAM-depleted mice (anti-CSF1R) as measured by bioluminescence (WT vehicle $n = 14$, WT TAM depletion $n = 5$, ΔCD24 vehicle $n = 13$, ΔCD24 TAM depletion $n = 5$. Two-way ANOVA with multiple comparisons correction, tumor genotype $F_{(3,33)} = 11.75$, *$P = 0.0296$, ***$P = 0.0009$). **c,** Survival analysis of vehicle-treated mice in **c,** P value computed by a log-rank (Mantel-Cox) test (WT $n = 5$, ΔCD24 $n = 5$). **d,** Representative bioluminescence image of Day 33 tumors in mice with MCF-7 tumors treated with either IgG control or anti-CD24 mAb (image representative of two experimental cohorts). Data are mean ±s.e.m. **e,** Burden of MCF-7 WT tumors treated with IgG control (blue) vs. anti-CD24 mAb (red) as measured by bioluminescence (IgG $n = 10$, anti-CD24 mAb $n = 10$. Days of anti-CD24 mAb administration indicated by arrows. Data of two experimental cohorts. Two-way ANOVA with multiple comparisons correction, tumor treatment $F_{(1,126)} = 5.679$, ****$P < 0.0001$).